

NUMERICAL ANALYSIS AND SCIENTIFIC COMPUTING
PREPRINT SERIA

**Superconvergence of discontinuous
Galerkin and local discontinuous
Galerkin methods: eigen-structure
analysis based on Fourier approach**

W. GUO X. ZHONG J. QIU

PREPRINT #18



DEPARTMENT OF MATHEMATICS
UNIVERSITY OF HOUSTON

OCTOBER 2013

Superconvergence of discontinuous Galerkin and local discontinuous Galerkin methods: eigen-structure analysis based on Fourier approach

Wei Guo ¹ Xinghui Zhong ² Jing-Mei Qiu³

Abstract

Various superconvergence properties of discontinuous Galerkin (DG) and local DG (LDG) methods for linear hyperbolic and parabolic equations have been investigated in the past. Due to these superconvergence properties, DG and LDG methods have been known to provide good wave resolution properties, especially for long time integrations [26]. In this paper, under the assumption of uniform mesh and via Fourier approach, we observe that the error of the DG or LDG solution can be decomposed into three parts: (1) dissipation and dispersion errors of the physically relevant eigenvalue; this part of error will grow linearly in time and is of order: $2k + 1$ for DG method and $2k + 2$ for LDG method (2) projection error: there exists a special projection of the exact solution such that the numerical solution is much closer to this special projection than the exact solution itself; this part of error will not grow in time (3) the dissipation of non-physically relevant eigenvectors; this part of error will be damped exponentially fast with respect to the spatial mesh size Δx . Along this line, we analyze the error for a fully discrete Runge-Kutta (RK) DG scheme. A collection of numerical examples for linear equations are presented to verify our observations above. We also provide numerical examples based on non-uniform mesh, nonlinear Burgers' equation, and high-dimensional Maxwell equations to explore superconvergence properties of DG methods in a more general setting.

Keywords: discontinuous Galerkin method, local discontinuous Galerkin method, Fourier approach, dispersion and dissipation error, eigen-structure, superconvergence

¹Department of Mathematics, University of Houston, Houston, 77004. E-mail: wguo126@math.uh.edu; Department of Mathematics, Nanjing University, Nanjing, Jiangsu 210093, PR China

²Division of Applied Mathematics, Brown University, Providence, 02912. E-mail: xzhong@dam.brown.edu

³Department of Mathematics, University of Houston, Houston, 77004. E-mail: jingqiu@math.uh.edu.

1 Introduction

In this paper, we investigate superconvergence properties of discontinuous Galerkin (DG) and local DG (LDG) methods for smooth solutions of linear hyperbolic and parabolic problems. DG and LDG methods are a class of finite element methods, designed for solving hyperbolic and parabolic problems among many others [10]. These methods use piecewise polynomial spaces of degree k that could be discontinuous across cell boundaries as solution and test function spaces. These methods have the advantage of being compact and flexible for unstructured meshes, and being suitable for h-p adaptivity. Moreover, it has been proved that both DG and LDG methods are of order $k + 1$ for linear problems with smooth enough solutions [10] for 1-D cases. For general meshes, DG solutions are proved to be $k + \frac{1}{2}$ order accurate for linear hyperbolic problems [18]. These methods also have some inherent dissipation mechanism for L^2 stability of nonlinear problems, see for example [14, 22] and references there in.

In this paper, our focus is on the superconvergence properties of DG and LDG solutions. Superconvergence properties of DG and LDG methods for hyperbolic and parabolic problems have been intensively investigated in the past. Lowrie et al. [17] discovered that when polynomials of degree k is used, “a component of error” of the DG method converges with order $2k + 1$ in L^2 norm. It is showed in [9, 16] that the DG and LDG solutions converge with order $2k + 1$ in terms of negative norm. Based on the negative norm estimate, the DG and LDG solutions on translation invariant grids can be post-processed via a kernel convolution with B-spline functions. The post-processed solution is proved to converge with order $2k + 1$ in L^2 norm [9, 19, 16]. Adjrid et al. in [1] analyzed the DG method in the setting of ordinary differential equations with the conclusion that the DG solution converges with order $k + 2$ at Radau points of each element, and with order $2k + 1$ at downwind points. In [2], Adjrid et al. numerically investigated the superconvergence of DG and LDG for convection-diffusion equations at Radau points. Cheng and Shu in [5, 6, 7] showed that the DG and LDG solution is closer to the Radau projection of the exact solution than the exact solution itself. As a result, the error of DG and LDG solution will not grow over a long time period $\mathcal{O}(\frac{1}{\sqrt{\Delta x}})$. In [13, 3, 4, 20, 21], Fourier analysis has been adopted to indicate the superconvergence properties of DG solution in terms of dispersion and dissipation error of physically relevant

eigenvalues. We remark that the work in [13, 3, 4] is based on initial-boundary value problem with a given inflow boundary condition, while our analysis in this paper is based on the initial-boundary value problem with a periodic boundary condition. Such difference leads to different assumptions, and therefore different observations and conclusions in the Fourier analysis. Zhong and Shu [26] use the Fourier analysis and symbolic computation to show that the DG method is superconvergent at Radau and downwind points with the order of $k + 2$ and $2k + 1$ respectively. In [23], for the first time that DG solutions are proved to converge at the optimal rate of $k + 2$ at Radau points under the general assumption of non-uniform mesh. Because of these superconvergence properties, the method is considered to be very competitive in resolving waves propagating with long time integrations.

Different approaches have been adopted to analyze the superconvergence properties of DG schemes, such as the negative norm estimate [9, 16], by considering the problem as an initial or boundary value problem [1, 13, 3, 4], by special decomposition of error and playing with test functions in the weak formulation [5, 23], Fourier analysis [26, 20, 21, 12] etc. Fourier analysis has been known to be limited to linear problems with periodic boundary conditions and uniform mesh. However, it provides a sufficient condition for instability of “bad” schemes [25] as well as a quantitative error estimate. It can be used as a guidance to results in a more general setting [26]. In this paper, we will continue adopting Fourier approach to analyze the errors of DG and LDG methods for time dependent linear hyperbolic and parabolic equations.

In this paper, we perform Fourier analysis and symbolically compute eigenvalues and the corresponding eigenvectors of the amplification matrices of the DG and LDG methods with P^k polynomial spaces. We obtain the following observations when $k = 1, 2, 3$:

1. There are $k + 1$ eigenvalues of the amplification matrices for DG and LDG schemes. One of these eigenvalues is physically relevant. It approximates the analytical wave propagation speed with an order of $2k + 1$ in dissipation error and an order of $2k + 2$ in dispersion error for DG solutions; and with an order of $2k + 2$ in dissipation error for LDG solutions. This is consistent with the results in [13, 3] for initial boundary value problems. The rest of the eigenvalues are non-physically relevant; they have large negative real part that is of order $\frac{1}{\Delta x}$ for DG and $\frac{1}{\Delta x^2}$ for LDG. As a result, the

corresponding non-physically relevant eigenvectors will be damped exponentially fast with respect to Δx over time.

2. There are $k + 1$ eigenvectors. If Lagrangian basis functions based on shifted Radau points are used, the eigenvector corresponding to the physically relevant eigenvalue approximates the wave function with order $k + 2$ at shifted Radau points and with order $2k + 1$ at downwind points.

Based on the observations above, we decompose the error of DG and LDG solutions into three parts. One part is due to the dissipation and dispersion errors of physically relevant eigenvalues; this part of error is of very high order ($2k + 1$ for DG and $2k + 2$ for LDG) and will grow linearly in time. The second part is the projection error from the eigenvector analysis. The magnitude of this part of error doesn't grow in time. The third part of error is related to how non-physically relevant eigenvectors are being dissipated over time. It is concluded in this paper that the error of the DG or LDG solution at Radau points will not grow over a period of time that is on the order of $\frac{1}{\Delta x^{k-1}}$ for DG solutions and is on the order of $\frac{1}{\Delta x^k}$ for LDG solutions, where k is the degree of polynomial space. We remark that the numerical solution is closer to the special projection investigated in this paper than that in [5].

The paper is organized as follows. In Section 2, a review of DG and LDG methods and Fourier approach is given. In Section 3, we symbolically analyze the eigenstructure of the amplification matrices of the DG (Section 3.1) and LDG (Section 3.2) schemes with polynomial degrees up to k ($1 \leq k \leq 3$). We also comment on the supraconvergence of DG scheme based on Radau points in Section 3.3. We analyze the fully discrete RKDG scheme in Section 3.4. In Section 4, numerical examples for scalar and system of equations in one and two spatial dimensions are provided to verify our theoretical results. Numerical examples on equations with variable coefficients, nonlinear equations, as well as schemes based on non-uniform meshes are also presented to assess superconvergence properties of DG and LDG schemes in a more general setting. Some interesting observations are discussed based on our understanding. Conclusions are given in Section 5.

2 DG and LDG scheme and Fourier analysis

2.1 DG scheme

We first review the DG formulation and Fourier analysis for the linear hyperbolic problem

$$\begin{aligned} u_t + au_x &= 0, \quad x \in [0, 2\pi], t > 0 \\ u(x, 0) &= \exp(i\omega x), \quad x \in [0, 2\pi] \end{aligned} \quad (2.1)$$

with periodic boundary conditions. Here a is a constant indicating wave propagation speed and ω is the wave number. For convenience, assume that $a > 0$.

To define the DG method for the model problem, we consider a uniform partition of the computational domain $[0, 2\pi]$ into N cells as follows:

$$0 = x_{\frac{1}{2}} < x_{\frac{3}{2}} < \cdots < x_{N+\frac{1}{2}} = 2\pi.$$

Denote the cell by $I_j = [x_{j-\frac{1}{2}}, x_{j+\frac{1}{2}}]$ and the cell center by $x_j = \frac{1}{2}(x_{j+\frac{1}{2}} + x_{j-\frac{1}{2}})$, for $j = 1, \dots, N$. Clearly, the cell size is $\Delta x = \frac{2\pi}{N}$. Define the approximation space as

$$V_h^k = \{v : v|_{I_j} \in P^k(I_j); 1 \leq j \leq N\} \quad (2.2)$$

where $P^k(I_j)$ denotes the set of polynomials of degree up to k defined on the cell I_j . The semi-discrete DG method using the upwind flux for solving (2.1) is defined as follows: find the unique function $u = u(\cdot, t) \in V_h^k$ such that, for all test functions $v \in V_h^k$, we have

$$\int_{I_j} u_t v \, dx - a \int_{I_j} uv_x \, dx + au_{j+\frac{1}{2}}^- v(x_{j+\frac{1}{2}}^-) - au_{j-\frac{1}{2}}^- v(x_{j-\frac{1}{2}}^+) = 0, \quad j = 1, \dots, N. \quad (2.3)$$

Here and below u^+ , u^- denote the left and right limits of the function u at the cell interface, respectively. Equation (2.3) is usually further discretized in time by a stable time integrator, such as the strong stability preserving (SSP) Runge-Kutta (RK) method [11].

To implement the scheme (2.3), we adopt a local basis of $P^k(I_j)$, denoted as

$$\{\phi_j^l(x), l = 1, 2, \dots, k+1\}. \quad (2.4)$$

Then the numerical solution can be represented as

$$u(x) = \sum_{l=1}^{k+1} u_j^l \phi_j^l(x), \quad x \in I_j. \quad (2.5)$$

After substituting (2.5) into (2.3) and inverting a local mass matrix, the DG scheme (2.3) can be written as

$$\frac{d\mathbf{u}_j}{dt} = \frac{a}{\Delta x} (A\mathbf{u}_j + B\mathbf{u}_{j-1}), \quad (2.6)$$

where $\mathbf{u}_j = (u_j^1, \dots, u_j^{k+1})^T$, A and B are $(k+1) \times (k+1)$ constant matrices.

Below we review the Fourier analysis [25, 26]. This analysis depends heavily on the assumption of uniform mesh and periodic boundary conditions. Assume

$$\mathbf{u}_j(t) = \hat{\mathbf{u}}(t) \exp(i\omega x_j), \quad (2.7)$$

substituting which into the DG scheme (2.6) provides the following ODE system for the coefficient vector $\hat{\mathbf{u}}(t)$,

$$\frac{d}{dt} \hat{\mathbf{u}}(t) = aG\hat{\mathbf{u}}(t), \quad (2.8)$$

where G is the amplification matrix, given by

$$G = \frac{1}{\Delta x} (A + B e^{-i\xi}), \quad \xi = \omega \Delta x. \quad (2.9)$$

If G is diagonalizable, denote the eigenvalues of G as $\lambda_1, \dots, \lambda_{k+1}$ and the corresponding eigenvectors as $\tilde{V}_1, \dots, \tilde{V}_{k+1}$. Then the general solution of the ODE system (2.8) is

$$\hat{\mathbf{u}}(t) = C_1 e^{a\lambda_1 t} \tilde{V}_1 + \dots + C_{k+1} e^{a\lambda_{k+1} t} \tilde{V}_{k+1}, \quad (2.10)$$

where C_1, \dots, C_{k+1} can be determined by the initial condition. Let $V_l = C_l \tilde{V}_l$, then

$$\hat{\mathbf{u}}(t) = e^{a\lambda_1 t} V_1 + \dots + e^{a\lambda_{k+1} t} V_{k+1}, \quad (2.11)$$

which is an explicit representation of DG solution for some future time $t > 0$.

2.2 LDG scheme

Below we review the LDG formulation and Fourier analysis for the linear parabolic problem

$$\begin{aligned} u_t - u_{xx} &= 0, \quad x \in [0, 2\pi], t > 0 \\ u(x, 0) &= \exp(i\omega x), \quad x \in [0, 2\pi] \end{aligned} \quad (2.12)$$

with periodic boundary conditions. The LDG scheme for (2.12) uses the same mesh and approximation space as those for the DG scheme in Section 2.1. It is formulated based on rewriting (2.12) as

$$\begin{aligned} u_t - q_x &= 0, \\ q - u_x &= 0. \end{aligned} \tag{2.13}$$

The scheme is defined as follows: find $u, q \in V_h^k$ such that, for all test functions $v, p \in V_h^k$ and $j = 1, \dots, N$, we have

$$\begin{aligned} \int_{I_j} u_t v \, dx + \int_{I_j} q v_x \, dx - \hat{q}_{j+\frac{1}{2}} v(x_{j+\frac{1}{2}}^-) + \hat{q}_{j-\frac{1}{2}} v(x_{j-\frac{1}{2}}^+) &= 0, \\ \int_{I_j} q p \, dx + \int_{I_j} u p_x \, dx - \hat{u}_{j+\frac{1}{2}} p(x_{j+\frac{1}{2}}^-) + \hat{u}_{j-\frac{1}{2}} p(x_{j-\frac{1}{2}}^+) &= 0, \end{aligned} \tag{2.14}$$

where a good choice for the fluxes \hat{q} and \hat{u} is

$$\hat{q} = q^+, \quad \hat{u} = u^-,$$

i.e. we alternately take the right and left limits for fluxes in q and u . The choice of $\hat{q} = q^-, \hat{u} = u^+$ is also fine.

Similar to the DG scheme, after choosing a set of local basis (2.4), the scheme (2.14) can be written as

$$\frac{d\mathbf{u}_j}{dt} = \frac{1}{\Delta x^2} (A_1 \mathbf{u}_{j-1} + B \mathbf{u}_j + A_2 \mathbf{u}_{j+1}), \tag{2.15}$$

where $\mathbf{u}_j = (u_j^1, \dots, u_j^{k+1})^T$, A_1 , B and A_2 are $(k+1) \times (k+1)$ constant matrices. Assume that the LDG solution is of the form in equation (2.7). Substituting (2.7) into (2.15) gives

$$\frac{d}{dt} \hat{\mathbf{u}}(t) = G \hat{\mathbf{u}}(t), \tag{2.16}$$

with the amplification matrix G given by

$$G = \frac{1}{\Delta x} (A_1 e^{-i\xi} + B + A_2 e^{i\xi}), \quad \xi = \omega \Delta x. \tag{2.17}$$

As in equation (2.11) for the DG solution, the explicit form of the LDG solution can also be expressed based on eigenvalues and eigenvectors of G in equation (2.17) if G is diagonalizable.

3 Eigen-structures of G: error estimate

3.1 DG scheme

3.1.1 1-D scalar and system of linear hyperbolic equations

Depending on different choices of basis functions in DG implementation, the amplification matrix G could be different. The eigenvalues of G however will stay the same, since the DG method is independent of the choice of basis functions. However, the eigenvectors will be basis-dependent. Below we analyze G matrix based on the basis functions that are the Lagrangian polynomials

$$\phi_j^l(x) = \prod_{i \neq l} \frac{x - x_j^i}{x_j^l - x_j^i}, \quad (3.1)$$

where

$$x_j^l = x_j + \frac{\zeta_{k,l}}{2} \Delta x, \quad l = 1, \dots, k+1,$$

are the $k+1$ shifted Radau points. $\{\zeta_{k,l}\}$ are the roots of the Radau polynomial $P_{k+1}(\zeta) - P_k(\zeta)$, where $P_k(\zeta)$ is the Legendre polynomial of degree k normalized such that

$$\int_{-1}^1 P_i(x) P_j(x) dx = \frac{2}{2i+1} \delta_{ij},$$

where δ_{ij} is the Kronecker delta. Such choice of basis functions will help to reveal the super-convergence properties at Radau and downwind points [1, 5].

Proposition 3.1. Consider DG methods with polynomial space P^k ($k = 1, 2, 3$) for linear hyperbolic problem (2.1) with uniform mesh. Consider Fourier analysis of the DG method using Lagrangian polynomials (3.1) based on shifted Radau points as basis functions. The amplification matrix G is diagonalizable with $k+1$ distinct eigenvalues. One of these eigenvalues denoted as λ_1 is the physically relevant one; it approximates the analytical value $-i\omega$ with dissipation error on the order of $2k+1$ and dispersion error on the order of $2k+2$. The rest of eigenvalues $\lambda_2, \dots, \lambda_{k+1}$ have negative real part with the magnitude on the order of $\frac{1}{\Delta x}$.

Proof. We perform symbolic computations via Mathematica to analyze eigenvalues of G . Here is a summary of our results:

- P^1 case

$$\lambda_1 = -i\omega - \frac{\omega^4}{72}\Delta x^3 - \frac{i\omega^5}{270}\Delta x^4 + \mathcal{O}(\Delta x^5)$$

$$\lambda_2 = -\frac{6}{\Delta x} + \mathcal{O}(1)$$

- P^2 case

$$\lambda_1 = -i\omega - \frac{\omega^6}{7200}\Delta x^5 - \frac{i\omega^7}{42000}\Delta x^6 + \mathcal{O}(\Delta x^7)$$

$$\lambda_{2,3} = \frac{-3 \pm \sqrt{51}i}{\Delta x} + \mathcal{O}(1)$$

- P^3 case

$$\lambda_1 = -i\omega - 7.08 \times 10^{-7}\omega^8\Delta x^7 - 9.00 \times 10^{-8}i\omega^9\Delta x^8 + \mathcal{O}(\Delta x^9)$$

$$\lambda_{2,3} = \frac{-0.42 \pm 6.61i}{\Delta x} + \mathcal{O}(1), \quad \lambda_4 = -\frac{19.15}{\Delta x} + \mathcal{O}(1)$$

It can be checked from above that for $k = 1, 2, 3$

$$\mathcal{R}(-i\omega - \lambda_1) = \mathcal{O}(\Delta x^{2k+1}), \quad \mathcal{I}(-i\omega - \lambda_1) = \mathcal{O}(\Delta x^{2k+2}).$$

$$\mathcal{R}(\lambda_l) < 0, \quad |\mathcal{R}(\lambda_l)| = \mathcal{O}\left(\frac{1}{\Delta x}\right), \quad l = 2, \dots, k+1.$$

■

Remark 3.2. The fact that the non-physically relevant eigenvalues have large negative real part on the order of $\frac{1}{\Delta x}$ indicates that the corresponding eigenvectors will be damped exponentially fast with respect to Δx over time.

Proposition 3.3. With the same assumption as Proposition 3.1, the eigenvector V_1 corresponding to the physically relevant eigenvalue λ_1 approximates $\hat{\mathbf{u}}(0)$ in equation (2.11) with order $k+2$ at Radau points and with order $2k+1$ at downwind points. The non-physically relevant eigenvectors V_l , $l = 2, \dots, k+1$ are of order $k+2$ at Radau points.

Proof. We perform symbolic computations via Mathematica. Below is a summary of our results:

- P^1 case

$$V_1 - \hat{\mathbf{u}}(0) = \begin{pmatrix} \frac{i\omega^3}{162}\Delta x^3 + \mathcal{O}(\Delta x^4) \\ -\frac{i\omega^3}{54}\Delta x^3 + \mathcal{O}(\Delta x^4) \end{pmatrix}$$

$$V_2 = \begin{pmatrix} -\frac{i\omega^3}{162}\Delta x^3 + \mathcal{O}(\Delta x^4) \\ \frac{i\omega^3}{54}\Delta x^3 + \mathcal{O}(\Delta x^4) \end{pmatrix}$$

- P^2 case

$$V_1 - \hat{\mathbf{u}}(0) = \begin{pmatrix} \frac{(3 + 8\sqrt{6})\omega^4}{20000}\Delta x^4 + \mathcal{O}(\Delta x^5) \\ \frac{(3 - 8\sqrt{6})\omega^4}{20000}\Delta x^4 + \mathcal{O}(\Delta x^5) \\ -\frac{i\omega^5}{3000}\Delta x^5 + \mathcal{O}(\Delta x^6) \end{pmatrix}$$

$$V_2 = \begin{pmatrix} -\frac{(153 + 408\sqrt{6} + i18\sqrt{34} - i29\sqrt{51})\omega^4}{2040000}\Delta x^4 + \mathcal{O}(\Delta x^5) \\ -\frac{(153 - 408\sqrt{6} - i18\sqrt{34} - i29\sqrt{51})\omega^4}{2040000}\Delta x^4 + \mathcal{O}(\Delta x^5) \\ -\frac{i\omega^4}{160\sqrt{51}}\Delta x^4 + \mathcal{O}(\Delta x^5) \end{pmatrix}$$

$$V_3 = \begin{pmatrix} -\frac{(153 + 408\sqrt{6} - i18\sqrt{34} + i29\sqrt{51})\omega^4}{2040000}\Delta x^4 + \mathcal{O}(\Delta x^5) \\ -\frac{(153 - 408\sqrt{6} + i18\sqrt{34} + i29\sqrt{51})\omega^4}{2040000}\Delta x^4 + \mathcal{O}(\Delta x^5) \\ \frac{i\omega^4}{160\sqrt{51}}\Delta x^4 + \mathcal{O}(\Delta x^5) \end{pmatrix}$$

- P^3 case

$$V_1 - \hat{\mathbf{u}}(0) = \begin{pmatrix} -4.58 \times 10^{-5}i\omega^5\Delta x^5 + \mathcal{O}(\Delta x^6) \\ 4.81 \times 10^{-5}i\omega^5\Delta x^5 + \mathcal{O}(\Delta x^6) \\ -2.61 \times 10^{-5}i\omega^5\Delta x^5 + \mathcal{O}(\Delta x^6) \\ -2.43 \times 10^{-6}i\omega^7\Delta x^7 + \mathcal{O}(\Delta x^8) \end{pmatrix}$$

$$\begin{aligned}
V_2 &= \begin{pmatrix} (2.13 \times 10^{-5} + i1.19 \times 10^{-5})\omega^5 \Delta x^5 + \mathcal{O}(\Delta x^6) \\ (1.55 \times 10^{-6} - i1.86 \times 10^{-5})\omega^5 \Delta x^5 + \mathcal{O}(\Delta x^6) \\ (-1.73 \times 10^{-5} + i9.61 \times 10^{-6})\omega^5 \Delta x^5 + \mathcal{O}(\Delta x^6) \\ (6.53 \times 10^{-6} + i2.31 \times 10^{-5})\omega^5 \Delta x^5 + \mathcal{O}(\Delta x^6) \end{pmatrix} \\
V_3 &= \begin{pmatrix} (-2.13 \times 10^{-5} + i1.19 \times 10^{-5})\omega^5 \Delta x^5 + \mathcal{O}(\Delta x^6) \\ (-1.55 \times 10^{-6} - i1.86 \times 10^{-5})\omega^5 \Delta x^5 + \mathcal{O}(\Delta x^6) \\ (1.73 \times 10^{-5} + i9.61 \times 10^{-6})\omega^5 \Delta x^5 + \mathcal{O}(\Delta x^6) \\ (-6.53 \times 10^{-6} + i2.31 \times 10^{-5})\omega^5 \Delta x^5 + \mathcal{O}(\Delta x^6) \end{pmatrix} \\
V_4 &= \begin{pmatrix} 2.20 \times 10^{-5}i\omega^5 \Delta x^5 + \mathcal{O}(\Delta x^6) \\ -1.09 \times 10^{-5}i\omega^5 \Delta x^5 + \mathcal{O}(\Delta x^6) \\ 6.85 \times 10^{-6}i\omega^5 \Delta x^5 + \mathcal{O}(\Delta x^6) \\ -4.62 \times 10^{-5}i\omega^5 \Delta x^5 + \mathcal{O}(\Delta x^6) \end{pmatrix}
\end{aligned}$$

Clearly, for $k = 1, 2, 3$, V_1 approximates $\hat{\mathbf{u}}(0)$ with order $2k + 1$ at downwind points and with order $k + 2$ at other Radau points. V_l , $l = 2, \dots, k + 1$ are of order $(k + 2)$ at Radau points. ■

Remark 3.4. We remark that the choice of Lagrangian basis functions based on shifted Radau points is crucial in estimating superconvergence properties at Radau points. If we choose other basis functions, e.g. Lagrangian basis functions based on uniformly distributed points as in [25], then the eigenvector V_1 approximates $\hat{\mathbf{u}}(0)$ with order $k + 1$ at all points, and V_l , $l \geq 2$, is of order $k + 1$ at all points. Details of symbolic computation are omitted for brevity.

Proposition 3.5. With the same assumption as Proposition 3.1, let $\mathbf{u}(T) = \hat{\mathbf{u}}(0)\exp(i\omega(x_j - aT))$ and $\mathbf{u}_h(T) = \hat{\mathbf{u}}(T)\exp(i\omega x_j)$ be point values of exact solution and numerical solution at shifted Radau points on a cell I_j . Let $\mathbf{e} = \mathbf{u} - \mathbf{u}_h$. Then for $T > 0$,

$$\|\mathbf{e}(T)\| \leq C_1 a T \Delta x^{2k+1} + C_2 \Delta x^{k+2} + C_3 \exp(-C \frac{aT}{\Delta x}) \Delta x^{k+2}, \quad (3.2)$$

where C, C_1, C_2, C_3 are positive constants independent of Δx and $\|\cdot\|$ can be any norm for vectors.

Proof. Note that in (2.11), $\hat{\mathbf{u}}(0) = \sum_{l=1}^{k+1} V_l$. By Equation (2.11), Proposition 3.1 and 3.3,

we have

$$\begin{aligned}
\|\mathbf{e}(T)\| &= \|\mathbf{u}(T) - \mathbf{u}_h(T)\| \\
&= \|\exp(-i\omega aT)\hat{\mathbf{u}}(0) - \sum_{l=1}^{k+1} \exp(\lambda_l aT)V_l\| \\
&\stackrel{(2.11)}{=} \|\exp(-i\omega aT)\sum_{l=1}^{k+1} V_l - \sum_{l=1}^{k+1} \exp(\lambda_l aT)V_l\| \\
&\leq \|(\exp(-i\omega aT) - \exp(\lambda_1 aT))V_1\| + |\exp(-i\omega aT)|\|\sum_{l=2}^{k+1} V_l\| + \sum_{l=2}^{k+1} \|\exp(\lambda_l aT)V_l\| \\
&\leq |\exp(-i\omega aT) - \exp(\lambda_1 aT)|\|V_1\| + \|\hat{\mathbf{u}}(0) - V_1\| + \sum_{l=2}^{k+1} |\exp(\lambda_l aT)|\|V_l\| \\
&\leq C_1 aT \Delta x^{2k+1} + C_2 \Delta x^{k+2} + C_3 \exp(-C \frac{aT}{\Delta x}) \Delta x^{k+2}
\end{aligned}$$

where C, C_1, C_2, C_3 are positive constants independent of Δx . Notice that $\|V_1\|$ is of order 1 by Proposition 3.3. ■

Remark 3.6. From Proposition 3.5, it can be seen that under the assumption of uniform mesh, the error of the DG solution for a linear hyperbolic problem can be decomposed as three parts:

1. Dissipation and dispersion errors of the physically relevant eigenvalue. This part of error will grow linearly in time and is of order $2k + 1$.
2. Projection error $\|\mathbf{u}^* - \mathbf{u}\|$. That is, there exists a special projection of the solution,

$$\mathbf{u}^*(T) = P_h^* \mathbf{u}(T) = \exp(i\omega(x_j - aT))V_1$$

on cell I_j , such that the numerical solution is much closer to the special projection of exact solution ($\|\mathbf{u}_h - \mathbf{u}^*\| = \mathcal{O}(\Delta x^{2k+1})$), than the exact solution itself. The projection error

$$\|\mathbf{u}^* - \mathbf{u}\| = \mathcal{O}(\Delta x^{k+2}),$$

will not grow in magnitude in time. By Proposition 3.3, such special projection approximates the exact solution at Radau points with order $k + 2$ with the exception of Radau point at downwind end, which is of order $2k + 1$. Unfortunately, the analytical

form of such special projection is only known symbolically and is subject to further investigation.

3. Dissipation of non-physically relevant eigenvectors. This part of error will decay exponentially fast over time with respect to Δx if $a \geq a_0 > 0$.

Remark 3.7. When $a > a_0 \geq 0$, the error $e(T)$ in Proposition 3.5 is of order $k + 2$ at Radau points and is of order $2k + 1$ at downwind points.

Remark 3.8. Based on the error estimate (3.2), one can conclude

(a) when $T = o(\frac{1}{\Delta x^{k-1}})$, $\mathcal{O}(\Delta x^{k+2})$ is the dominant term in (3.2); this term will not grow with time;

(b) when $T = \mathcal{O}(\frac{1}{\Delta x^{k-1}})$ (very long time integration), $C_1 a T \Delta x^{2k+1}$ is the dominant term in (3.2); this term grows linearly with time and is of order $2k + 1$.

Since it is hard to check numerically the long time behavior of the error of DG solutions, we propose to use the following Corollary as a way to numerically assess our theoretical results discussed in this section.

Corollary 3.9. Consider DG methods with polynomial space P^k ($k = 1, 2, 3$) for linear problem (2.1) with uniform mesh. Let $n > 1$ be an integer, then

$$\|\mathbf{u}_h(t + \frac{2n\pi}{a}) - \mathbf{u}_h(t)\| \leq C_1 n (\Delta x^{2k+1}) + C_2 \exp(-\frac{Cat}{\Delta x}) \Delta x^{k+2}, \quad (3.3)$$

where C , C_1 and C_2 are positive constants independent of Δx .

Proof.

$$\begin{aligned} \|\mathbf{u}_h(t + \frac{2n\pi}{a}) - \mathbf{u}_h(t)\| &= \left\| \sum_{l=1}^{k+1} (\exp(\lambda_l(at + 2n\pi)) - \exp(\lambda_l at)) V_l \right\| \\ &\leq |\exp(\lambda_1(at + 2n\pi)) - \exp(\lambda_1 at)| \|V_1\| \\ &\quad + \sum_{l=2}^{k+1} |\exp(\lambda_l(at + 2n\pi)) - \exp(\lambda_l at)| \|V_l\| \\ &\leq |\exp(\lambda_1 2n\pi) - \exp(i\omega 2n\pi)| |\exp(\lambda_1 at)| \|V_1\| + C_2 \exp(-\frac{Cat}{\Delta x}) \Delta x^{k+2} \\ &\leq C_1 n |\lambda_1 - i\omega| + C_2 \exp(-\frac{Cat}{\Delta x}) \Delta x^{k+2} \\ &\leq C_1 n \Delta x^{2k+1} + C_2 \exp(-\frac{Cat}{\Delta x}) \Delta x^{k+2}. \end{aligned}$$

■

Remark 3.10. Assume $a = 1$, let $T = 2n\pi + t$ with $t = \mathcal{O}(1)$, then the first term on the r.h.s. of (3.3) is the dominant term.

$$\begin{aligned} \|e(T)\| &= \|\mathbf{u}(T) - \mathbf{u}_h(T)\| \\ &= \|\mathbf{u}(t) - \mathbf{u}_h(2n\pi + t)\| \\ &\leq \|\mathbf{u}_h(2n\pi + t) - \mathbf{u}_h(t)\| + \|\mathbf{u}(t) - \mathbf{u}_h(t)\|. \end{aligned}$$

Since $\|\mathbf{u}_h(2n\pi + t) - \mathbf{u}_h(t)\|$ is order of $2k + 1$ and grows linearly with n , we can conclude that the error $e(T)$ will not grow linearly in time until $T = \mathcal{O}(\frac{1}{\Delta x^{k-1}})$.

Remark 3.11. When a is of order 1, the dominant error on the r.h.s. of (3.3) is of order $2k + 1$. This observation is numerically verified in many examples presented in Section 4. When a is very small, the dominant error is of order $k+2$, rather than $2k+1$. This observation is important in explaining the numerical performance of DG schemes for a nonlinear Burgers equation in Example 4.4 and for a rotational problem in Example 4.8.

Remark 3.12. Proposition 3.5 and Corollary 3.9 can be extended to a linear hyperbolic system $U_t + AU_x = 0$, where $A_{n \times n}$ is a constant diagonalizable matrix with real eigenvalues. This is due to the fact that the hyperbolic system can be decoupled to n scalar equations.

3.1.2 DG scheme for 2-D problem: Q^k

In this subsection, we analyze the DG method for a 2-D linear advection equation

$$u_t + au_x + bu_y = 0, \quad (x, y) \in [0, 2\pi]^2 \quad (3.4)$$

via Fourier analysis. Without loss of generality, we assume that $a, b > 0$. Consider a uniform partition of the computational domain as $[0, 2\pi]^2 = \cup_{i,j} I_{ij} = \cup_{i,j} [x_{i-\frac{1}{2}}, x_{i+\frac{1}{2}}] \times [y_{j-\frac{1}{2}}, y_{j+\frac{1}{2}}]$. The basis functions are chosen to be 2-D functions Q^k which are tensor products of 1-D ones on each cell I_{ij} . Define the approximation space

$$V_h^k = \{v : v|_{I_{ij}} \in Q^k(I_{ij}); 1 \leq i \leq N, 1 \leq j \leq N\}. \quad (3.5)$$

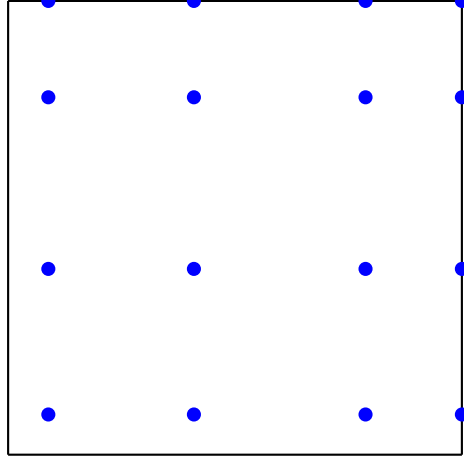


Figure 3.1: Radau points in two-dimensional case.

The semi-discrete DG method using the upwind flux for solving (3.4) is defined as follows: find $u(\cdot, \cdot, t) \in V_h^k$, such that

$$\begin{aligned}
 \int_{I_{ij}} u_t v \, dx dy = & \quad a \int_{I_{ij}} uv_x \, dx dy + b \int_{I_{ij}} uv_y \, dx dy & (3.6) \\
 & - a \left(\int_{y_{j-\frac{1}{2}}}^{y_{j+\frac{1}{2}}} u_{i+\frac{1}{2},j}^-(y) v(x_{i+\frac{1}{2}}^-, y) \, dy - \int_{y_{j-\frac{1}{2}}}^{y_{j+\frac{1}{2}}} u_{i-\frac{1}{2},j}^-(y) v(x_{i-\frac{1}{2}}^+, y) \, dy \right) \\
 & - b \left(\int_{x_{i-\frac{1}{2}}}^{x_{i+\frac{1}{2}}} u_{i,j+\frac{1}{2}}^-(x) v(x, y_{j+\frac{1}{2}}^-) \, dx - \int_{x_{i-\frac{1}{2}}}^{x_{i+\frac{1}{2}}} u_{i,j-\frac{1}{2}}^-(x) v(x, y_{j-\frac{1}{2}}^+) \, dx \right)
 \end{aligned}$$

for all $v \in V_h^k$. As in 1-D case, to illustrate the superconvergence properties at Radau nodes, we use the following basis functions

$$B_{m,n} = L_m(x)L_n(y), \quad m, n = 1, \dots, k+1$$

where $L_m(x)$ and $L_n(y)$ are shifted Radau Lagrangian basis functions (3.1) in x - and y -directions respectively. Please see Figure 3.1 for distribution of shifted Radau points in a cell.

In the Fourier analysis, the DG solution is assumed to be of the form

$$\mathbf{u}(t) = \hat{\mathbf{u}}(t) \exp(i\omega_x x_i + i\omega_y y_j), \quad (3.7)$$

where $\hat{\mathbf{u}}(t)$ is the coefficient vector of $(k+1)^2$ elements. We substitute equation (3.7) into the DG scheme (3.6) to obtain an ODE system for the coefficient vector

$$\frac{d}{dt} \hat{\mathbf{u}}(t) = G \hat{\mathbf{u}}(t).$$

Let G^{x,ω_x} and G^{y,ω_y} be the 1-D amplification matrix in x - and y - direction respectively. Then the 2-D amplification matrix G can be written as

$$G = aI \otimes G^{x,\omega_x} + bG^{y,\omega_y} \otimes I, \quad (3.8)$$

where \otimes is the tensor product or Kronecker product of two matrices.

Proposition 3.13. The 2-D amplification matrix G in equation (3.8) has $(k+1)^2$ eigenvalues,

$$a\lambda^{x,(p)} + b\lambda^{y,(q)}, \quad p, q = 1, \dots, k+1$$

with the corresponding eigenvectors

$$V^{y,(q)} \otimes V^{x,(p)},$$

where $\lambda^{x,(p)}$ and $V^{x,(p)}$, $p = 1, \dots, k+1$, $\lambda^{y,(q)}$ and $V^{y,(q)}$, $q = 1, \dots, k+1$ are eigenvalues and eigenvectors for G^{x,ω_x} and G^{y,ω_y} respectively.

Proof. Since $(A \otimes B)(\mathbf{x} \otimes \mathbf{y}) = A\mathbf{x} \otimes B\mathbf{y}$, we have

$$\begin{aligned} G(V^{y,(q)} \otimes V^{x,(p)}) &= (aI \otimes G^{x,\omega_x} + bG^{y,\omega_y} \otimes I)(V^{y,(q)} \otimes V^{x,(p)}) \\ &= aV^{y,(q)} \otimes (G^{x,\omega_x} V^{x,(p)}) + bG^{y,\omega_y} V^{y,(q)} \otimes V^{x,(p)} \\ &= a\lambda^{x,(p)}(V^{y,(q)} \otimes V^{x,(p)}) + b\lambda^{y,(q)}(V^{y,(q)} \otimes V^{x,(p)}) \\ &= (a\lambda^{x,(p)} + b\lambda^{y,(q)})(V^{y,(q)} \otimes V^{x,(p)}). \end{aligned}$$

■

Similar to the 1-D case, based on our understanding on the eigen-structures of 2-D amplification matrices, we have the following error estimate for the DG method with Q^k basis functions for a 2-D linear advection problem (3.4). The proof is similar to the 1-D case, and thus is omitted.

Proposition 3.14. Consider DG methods with polynomial space Q^k ($k = 1, 2, 3$) for a 2-D linear hyperbolic problem (3.4) with uniform mesh size Δx and Δy in x - and y - directions respectively. Let $\mathbf{u}(T) = \hat{\mathbf{u}}(0)\exp(i\omega_x(x_i - aT) + i\omega_y(y_j - bT))$ and $\mathbf{u}_h(T) = \hat{\mathbf{u}}(T)\exp(i\omega_x x_j +$

$i\omega_y y_j$) be point values of exact and numerical solution at shifted Radau points in a cell I_{ij} .

Let $\mathbf{e} = \mathbf{u} - \mathbf{u}_h$, then for $T > 0$,

$$\|\mathbf{e}(T)\| \leq C_1 T (a\Delta x^{2k+1} + b\Delta y^{2k+1}) + C_2 (\Delta x^{k+2} + \Delta y^{k+2}) + C_3 \exp(-CT(\frac{a}{\Delta x} + \frac{b}{\Delta y})) (\Delta x^{k+2} + \Delta y^{k+2}), \quad (3.9)$$

where C, C_1, C_2, C_3 are positive constants independent of Δx and Δy .

Remark 3.15. Consider a DG method for a 2-D linear problem (3.4) using polynomial spaces

$$P^k(I_{ij}) = \left\{ \sum_{i+j \leq k} c_{ij} x^i y^j \right\} \quad (3.10)$$

as polynomials up to degree k on each cell I_{ij} . Unlike the Q^k case, the eigen-structure for a 2-D amplification matrix cannot be analyzed via our understanding on a 1-D case, since the number of basis functions increase quadratically with k and it is difficult to obtain the roots of an algebraic equation of degree higher than 4.

3.2 LDG scheme

In this subsection, we discuss the eigen-structure of the amplification matrix from an LDG scheme for linear parabolic problem (2.12). As in a DG scheme, we formulate the amplification matrix with Lagrangian basis functions (3.1) based on the $k + 1$ shifted Radau points. Such choice of basis functions will help to reveal superconvergence properties at Radau points [2, 6]. The direction of the Radau points is determined by the choice of the numerical flux. In the following analysis and simulation, we choose $\hat{u} = u^-$ and $\hat{q} = q^+$. In this case, the right-shifted Radau points are used and the corresponding downwind points are $x_{j+\frac{1}{2}}^-$. Note that the amplification matrix of the LDG scheme for equation (2.12) can be derived from the amplification matrix of DG scheme for equation (2.1) with $a = 1$ directly. Specifically, let G_{DG} and G_{LDG} denote the amplification matrix of DG and LDG respectively. Then

$$G_{LDG} = -W\bar{G}_{DG}WG_{DG}. \quad (3.11)$$

Here \bar{G}_{DG} is the conjugate of G_{DG} , i.e.

$$G_{DG} = \frac{1}{\Delta x} (A + Be^{-i\xi}), \quad \bar{G}_{DG} = \frac{1}{\Delta x} (A + Be^{i\xi}),$$

with the notations introduced in (2.9). W is the change of basis matrix, which maps function values at right-shifted Radau points to the left-shifted ones. By the symmetry of right-shifted and left-shifted Radau points distribution, W features the property $W^{-1} = W$. For example, for P^1 case, the right-shifted Radau points are ordered as $(x_{j-\frac{1}{6}}, x_{j+\frac{1}{2}})$, the left-shifted ones are ordered as $(x_{j+\frac{1}{6}}, x_{j-\frac{1}{2}})$, and

$$W = \begin{pmatrix} \frac{1}{2} & \frac{1}{2} \\ \frac{3}{2} & -\frac{1}{2} \end{pmatrix}.$$

Notice the symmetry of these two set of points with respect to x_j . Due to such symmetry, it can be checked that $W^{-1} = W$ as claimed above.

Proposition 3.16. Consider LDG methods with polynomial space P^k ($k = 1, 2, 3$) for linear parabolic problem (2.12) with uniform mesh. Consider Fourier analysis of the LDG method using Lagrangian basis functions (3.1) based on shifted Radau points. The amplification matrix G is diagonalizable with $(k+1)$ distinct eigenvalues. One of these eigenvalues denoted as λ_1 is the physically relevant one, approximating $-\omega^2$ with dissipation error on the order of $2k+2$. The rest of eigenvalues $\lambda_2, \dots, \lambda_{k+1}$ have negative real part with the magnitude on the order of $\frac{1}{\Delta x^2}$.

Proof. We perform symbolic computations on Mathematica. Below is a summary of eigenvalues of G .

- P^1 case

$$\lambda_1 = -\omega^2 + \frac{\omega^6}{540}\Delta x^4 + \frac{11\omega^8}{108864}\Delta x^6 + \mathcal{O}(\Delta x^8)$$

$$\lambda_2 = -\frac{36}{\Delta x^2} + \mathcal{O}(1)$$

- P^2 case

$$\lambda_1 = -\omega^2 + \frac{\omega^8}{128000}\Delta x^6 + \frac{\omega^{10}}{8100000}\Delta x^8 + \mathcal{O}(\Delta x^{10})$$

$$\lambda_{2,3} = \frac{-78 \pm 6\sqrt{69}}{\Delta x^2} + \mathcal{O}(1)$$

- P^3 case

$$\lambda_1 = -\omega^2 - 2.25 \times 10^{-8} \omega^{10} \Delta x^8 - 7.51 \times 10^{-11} \omega^{12} \Delta x^{10} + \mathcal{O}(\Delta x^{12})$$

$$\lambda_2 = -\frac{438.91}{\Delta x^2} + \mathcal{O}(1)$$

$$\lambda_3 = -\frac{46.58}{\Delta x^2} + \mathcal{O}(1)$$

$$\lambda_4 = -\frac{34.51}{\Delta x^2} + \mathcal{O}(1)$$

It can be checked from above that for $k = 1, 2, 3$

$$\mathcal{R}(-\omega^2 - \lambda_1) = \mathcal{O}(\Delta x^{2k+2}).$$

$$\mathcal{R}(\lambda_l) < 0, \quad |\mathcal{R}(\lambda_l)| = \mathcal{O}\left(\frac{1}{\Delta x^2}\right), \quad l = 2, \dots, k+1.$$

■

Remark 3.17. In our symbolic computation, we find that the eigenvalues of the amplification matrix G for LDG methods are real for $k = 1, 2, 3$. However, this fact is difficult to prove based on equation (3.11).

Remark 3.18. The fact that the other eigenvalues have large negative real part on the order of $\frac{1}{\Delta x^2}$ indicates that the corresponding errors will be damped out exponentially fast with respect to Δx over time.

Proposition 3.19. With the same assumption as Proposition 3.16, the eigenvector V_1 corresponding to the physically relevant eigenvalue λ_1 approximates $\hat{\mathbf{u}}(0)$ with order $k+2$ at Radau points and with order $2k+1$ at downwind points. The non-physically relevant eigenvectors V_l , $l = 2, \dots, k+1$ are of order $k+2$ at Radau points.

Proof. We perform symbolic computations on Mathematica. Below is a summary of our results.

- P^1 case

$$V_1 - \hat{\mathbf{u}}(0) = \begin{pmatrix} -\frac{i\omega^3}{324} \Delta x^3 + \mathcal{O}(\Delta x^4) \\ \frac{i\omega^3}{108} \Delta x^3 + \mathcal{O}(\Delta x^4) \end{pmatrix}$$

$$V_2 = \begin{pmatrix} \frac{i\omega^3}{324}\Delta x^3 + \mathcal{O}(\Delta x^4) \\ -\frac{i\omega^3}{108}\Delta x^3 + \mathcal{O}(\Delta x^4) \end{pmatrix}$$

• P^2 case

$$V_1 - \hat{\mathbf{u}}(0) = \begin{pmatrix} -\frac{(3 + 8\sqrt{6})\omega^4}{60000}\Delta x^4 + \mathcal{O}(\Delta x^5) \\ -\frac{(3 - 8\sqrt{6})\omega^4}{60000}\Delta x^4 + \mathcal{O}(\Delta x^5) \\ -\frac{i\omega^5}{18000}\Delta x^5 + \mathcal{O}(\Delta x^6) \end{pmatrix}$$

$$V_2 = \begin{pmatrix} \frac{(207 + 552\sqrt{6} + 162\sqrt{46} - 11\sqrt{69})\omega^4}{8280000}\Delta x^4 + \mathcal{O}(\Delta x^5) \\ \frac{(207 - 552\sqrt{6} - 162\sqrt{46} + 11\sqrt{69})\omega^4}{8280000}\Delta x^4 + \mathcal{O}(\Delta x^5) \\ \frac{\omega^4}{480\sqrt{69}}\Delta x^4 + \mathcal{O}(\Delta x^5) \end{pmatrix}$$

$$V_3 = \begin{pmatrix} \frac{(207 + 552\sqrt{6} - 162\sqrt{46} + 11\sqrt{69})\omega^4}{8280000}\Delta x^4 + \mathcal{O}(\Delta x^5) \\ \frac{(207 - 552\sqrt{6} + 162\sqrt{46} - 11\sqrt{69})\omega^4}{8280000}\Delta x^4 + \mathcal{O}(\Delta x^5) \\ -\frac{\omega^4}{480\sqrt{69}}\Delta x^4 + \mathcal{O}(\Delta x^5) \end{pmatrix}$$

• P^3 case

$$V_1 - \hat{\mathbf{u}}(0) = \begin{pmatrix} 1.15 \times 10^{-5}i\omega^5\Delta x^5 + \mathcal{O}(\Delta x^6) \\ -1.20 \times 10^{-5}i\omega^5\Delta x^5 + \mathcal{O}(\Delta x^6) \\ 6.52 \times 10^{-6}i\omega^5\Delta x^5 + \mathcal{O}(\Delta x^6) \\ 4.05 \times 10^{-7}i\omega^7\Delta x^7 + \mathcal{O}(\Delta x^8) \end{pmatrix}$$

$$V_2 = \begin{pmatrix} -3.06 \times 10^{-6}i\omega^5\Delta x^5 + \mathcal{O}(\Delta x^6) \\ -1.20 \times 10^{-5}i\omega^5\Delta x^5 + \mathcal{O}(\Delta x^6) \\ -7.02 \times 10^{-7}i\omega^5\Delta x^5 + \mathcal{O}(\Delta x^6) \\ 1.19 \times 10^{-5}i\omega^5\Delta x^5 + \mathcal{O}(\Delta x^6) \end{pmatrix}$$

$$V_3 = \begin{pmatrix} -5.96 \times 10^{-6} i \omega^5 \Delta x^5 + \mathcal{O}(\Delta x^6) \\ 1.24 \times 10^{-6} i \omega^5 \Delta x^5 + \mathcal{O}(\Delta x^6) \\ 3.40 \times 10^{-6} i \omega^5 \Delta x^5 + \mathcal{O}(\Delta x^6) \\ -4.61 \times 10^{-6} i \omega^5 \Delta x^5 + \mathcal{O}(\Delta x^6) \end{pmatrix}$$

$$V_4 = \begin{pmatrix} -2.45 \times 10^{-6} i \omega^5 \Delta x^5 + \mathcal{O}(\Delta x^6) \\ 1.04 \times 10^{-5} i \omega^5 \Delta x^5 + \mathcal{O}(\Delta x^6) \\ -9.22 \times 10^{-6} i \omega^5 \Delta x^5 + \mathcal{O}(\Delta x^6) \\ -7.31 \times 10^{-6} i \omega^5 \Delta x^5 + \mathcal{O}(\Delta x^6) \end{pmatrix}$$

It can be checked that for $k = 1, 2, 3$, V_1 approximates $\hat{\mathbf{u}}(0)$ with order $2k + 1$ at downwind points and with order $k + 2$ at other Radau points. V_l , $l = 2, \dots, k + 1$ are of order $(k + 2)$ at Radau points. ■

Proposition 3.20. Consider LDG methods with polynomial space P^k ($k = 1, 2, 3$) for the linear parabolic problem (2.12) with uniform mesh. Let $\mathbf{u}(T) = \hat{\mathbf{u}}(0) \exp(i\omega x_j - \omega^2 T)$ and $\mathbf{u}_h(T) = \hat{\mathbf{u}}(T) \exp(i\omega x_j)$ be point values of exact and LDG solutions at shifted Radau points on a cell I_j . Let $\mathbf{e} = \mathbf{u} - \mathbf{u}_h$, then for $T > 0$,

$$\|\mathbf{e}(T)\| \leq C_1 T \Delta x^{2k+2} + C_2 \Delta x^{k+2} + C_3 \exp(-C \frac{T}{\Delta x^2}) \Delta x^{k+2}, \quad (3.12)$$

where C, C_1, C_2, C_3 are positive constants independent of Δx .

Proof. The result can be derived based on Proposition 3.16 and 3.19. The proof is similar to Proposition 3.5.

Remark 3.21. Similar to the case of DG scheme, the error of the LDG solution can be decomposed as three parts:

- (a) Dissipation error of the physically relevant eigenvalue in the order of $2k + 2$;
- (b) Projection error $\|\mathbf{u}^* - \mathbf{u}\|$: the numerical solution is much closer to the special projection of exact solution denoted as \mathbf{u}^* ($\|\mathbf{u}^* - \mathbf{u}_h\| = \mathcal{O}(\Delta x^{2k+2})$), than the exact solution itself ($\|\mathbf{u} - \mathbf{u}_h\| = \mathcal{O}(\Delta x^{k+2})$);
- (c) Dissipation of non-physically relevant eigenvectors.

Remark 3.22. Based on the error estimate (3.12), one can conclude

(a) when $T = o(\frac{1}{\Delta x^k})$, $\mathcal{O}(\Delta x^{k+2})$ is the dominant term in (3.12); this term will not grow with time;

(b) when $T = \mathcal{O}(\frac{1}{\Delta x^k})$, $\mathcal{O}(\Delta x^{2k+2})T$ is the dominant term in (3.12); this term grows linearly with time and is of order $2k + 2$.

As for the DG scheme, it is hard to check numerically the long time behavior of the error of LDG solutions, we propose to use the following corollary as a way to numerically assess our theoretical results above. Our numerical results on LDG method in the next section is based on the following corollary.

Corollary 3.23. Consider LDG methods with polynomial space P^k ($k = 1, 2, 3$) for linear parabolic problem (2.12) with uniform mesh. Let $T > t$ and $t = \mathcal{O}(1)$, then

$$\|\mathbf{u}_h(T) - \mathbf{u}_h(t)\exp(-\omega^2(T-t))\| \leq C_1(T-t)\Delta x^{2k+2} + C_2\exp(-\frac{Ct}{\Delta x^2})\Delta x^{k+2},$$

where C , C_1 and C_2 are positive constants independent of Δx .

Proof. The proof is similar to Corollary 3.9.

$$\begin{aligned} \|\mathbf{u}_h(T) - \mathbf{u}_h(t)\exp(-\omega^2(T-t))\| &= \left\| \sum_{l=1}^{k+1} (\exp(\lambda_l T) - \exp(\lambda_l t - (T-t)\omega^2))V_l \right\| \\ &\leq \|\exp(\lambda_1 T) - \exp(\lambda_1 t - \omega^2(T-t))\| \|V_1\| \\ &\quad + \left\| \sum_{l=2}^{k+1} (\exp(\lambda_l T) - \exp(\lambda_l t - \omega^2(T-t))) \right\| \|V_l\| \\ &\leq |\exp(\lambda_1(T-t) - \exp(-\omega^2(T-t)))\exp(\lambda_1 t)| \|V_1\| \\ &\quad + C_2\exp(-\frac{Ct}{\Delta x^2})\Delta x^{k+2} \\ &\leq C_1(T-t)\Delta x^{2k+2} + C_2\exp(-\frac{Ct}{\Delta x^2})\Delta x^{k+2} \end{aligned}$$

■

Remark 3.24. Similar to Remark 3.10, let $T > t$ and $t = \mathcal{O}(1)$, then

$$\begin{aligned} \|e(T)\| &= \|\mathbf{u}(T) - \mathbf{u}_h(T)\| \\ &= \|\exp(-w^2(T-t))\mathbf{u}(t) - \mathbf{u}_h(T)\| \\ &\leq \|\mathbf{u}_h(T) - \exp(-w^2(T-t))\mathbf{u}_h(t)\| + |\exp(-w^2(T-t))| \|\mathbf{u}(t) - \mathbf{u}_h(t)\| \\ &\leq \|\mathbf{u}_h(T) - \exp(-w^2(T-t))\mathbf{u}_h(t)\| + \|\mathbf{u}(t) - \mathbf{u}_h(t)\|. \end{aligned}$$

From Corollary 3.23, the dominant term in $\|\mathbf{u}_h(2n\pi + t) - \exp(-w^2(T - t))\mathbf{u}_h(t)\|$ is order of $2k + 2$. Thus the error $e(T)$ of LDG scheme will not grow until $T = \mathcal{O}(\frac{1}{\Delta x^k})$.

3.3 Supraconvergence of DG and LDG scheme

In [24], a so-called supraconvergence property of the DG scheme was studied. It was discovered that the leading term of the local truncation error for the DG scheme is first order accurate when piecewise P^1 polynomial is used with basis functions being Lagrangian interpolant based on uniformly distributed points (i.e. $\phi_{j-\frac{1}{4}}$ and $\phi_{j+\frac{1}{4}}$). In this section, we further study the supraconvergence property of the DG and LDG scheme based on our analysis for the eigen-structure of amplification matrices G .

Firstly, we look into the DG scheme for the model problem (2.1). Without loss of generality, we assume that $a = 1$. Denote D to be the temporal differentiation operator of $\hat{\mathbf{u}}(0)$ with $D\hat{\mathbf{u}}(0) = -i\omega\hat{\mathbf{u}}(0)$. Then the local truncation error denoted as LTE satisfies

$$LTE = D\hat{\mathbf{u}}(0) - G\hat{\mathbf{u}}(0). \quad (3.13)$$

Keeping the notation in equation (2.11), we have

$$\begin{aligned} LTE &= D\hat{\mathbf{u}}(0) - G\hat{\mathbf{u}}(0) \\ &= (-i\omega - \lambda_1)V_1 - \sum_{l=2}^{k+1}(\lambda_l + i\omega)V_l \end{aligned}$$

From our analysis in Section 3.1, we have $(-i\omega - \lambda_1)V_1 = \mathcal{O}(\Delta x^{2k+1})$, $(\lambda_l + i\omega) = \mathcal{O}(\Delta x^{-1})$ and $V_l = \mathcal{O}(\Delta x^{k+2})$ for $l \geq 2$ where $k = 1, 2, 3$. Thus the LTE based on shifted Radau points is obtained as:

$$LTE = \mathcal{O}(\Delta x^{k+1}). \quad (3.14)$$

It is observed that, due to our estimate for $\lambda_l = \mathcal{O}(\Delta x^{-1})$ with $l \geq 2$, the order of local truncation error is one order lower than the error in (3.2). Note that the local truncation error analyzed based on uniformly distributed points [24] is one order lower than that based on shifted Radau points (3.14). This fact partially explains the supraconvergence property of DG scheme discussed in [24].

Similar results can be derived for LDG schemes.

$$\begin{aligned}
LTE &= D^2\hat{\mathbf{u}}(0) - G\hat{\mathbf{u}}(0) \\
&= (-\omega^2 - \lambda_1)V_1 - \sum_{l=2}^{k+1}(\lambda_l + \omega^2)V_l \\
&= \mathcal{O}(\Delta x^k)
\end{aligned} \tag{3.15}$$

since $-\omega^2 - \lambda_1 = \mathcal{O}(\Delta x^{2k+2})$, $(\lambda_l + \omega^2) = \mathcal{O}(\Delta x^{-2})$ and $V_l = \mathcal{O}(\Delta x^{k+2})$ for $l \geq 2$, when $k = 1, 2, 3$. The order of local truncation error is two orders lower than the error in equation (3.12) based on shifted Radau points. Similarly, when uniformly distributed Lagrangian basis is used, we have $LTE = \mathcal{O}(\Delta x^{k-1})$.

3.4 Fully discrete schemes

An analysis of fully discretized RKDG schemes will be presented below. Without loss of generality, assume $a = 1$ in (2.3).

Let \tilde{u} be the approximation solution of the fully discretized version of (2.3) obtained by using an explicit RK methods of order p [11]. Denote $\tilde{\mathbf{u}}_n(T) = \tilde{\mathbf{u}}^n \exp(i\omega x_j)$ to be the point values of the solution \tilde{u} at shifted Radau points on a cell I_j at time T . Then

$$\tilde{\mathbf{u}}^n = R^n \hat{\mathbf{u}}(0), \quad n = \frac{T}{\Delta t},$$

with

$$R = 1 + \Delta t G + \frac{\Delta t^2}{2!} G^2 + \dots + \frac{\Delta t^p}{p!} G^p \tag{3.16}$$

for an explicit p^{th} order RK method, where the amplification matrix G is defined in (2.9). Consider the eigen-structure of $G = Q\Lambda Q^{-1}$, where $Q = [V_1, \dots, V_{k+1}]$ is the matrix with its columns being G 's eigenvectors and $\Lambda = \text{diag}(\lambda_1, \dots, \lambda_{k+1})$ where λ_i , $i = 1, \dots, k+1$ are G 's eigenvalues, then

$$\tilde{\mathbf{u}}^n = \sum_{l=1}^{k+1} \left(1 + \Delta t \lambda_l + \dots + \frac{\Delta t^p}{p!} \lambda_l^p \right)^n V_l \tag{3.17}$$

Proposition 3.25. With the same assumption as Proposition 3.5. Denote $\tilde{\mathbf{u}}_n$ as the numerical solution of fully discretized DG scheme with k^{th} order polynomial as solutions space

and with p^{th} order RK method. Let $\tilde{\mathbf{e}} = \mathbf{u} - \tilde{\mathbf{u}}_h$. Then for $T > 0$, and under certain linear stability constrain for time step Δt , we have the error estimate

$$\|\tilde{\mathbf{e}}(T)\| \leq C_1 T \Delta x^{2k+1} + C_2 \Delta x^{k+2} + C_3 T \Delta t^p, \quad (3.18)$$

where C_1, C_2, C_3 are positive constants independent of Δx and Δt . Here $\|\cdot\|$ can be any norm for vectors.

Proof.

$$\|\tilde{\mathbf{e}}(T)\| = \|\mathbf{u}(T) - \tilde{\mathbf{u}}_h(T)\| \leq \|\mathbf{u}(T) - \mathbf{u}_h(T)\| + \|\mathbf{u}_h(T) - \tilde{\mathbf{u}}_h(T)\| \quad (3.19)$$

By Proposition 3.5 with $a = 1$, we have

$$\|\mathbf{u}(T) - \mathbf{u}_h(T)\| \leq C_1 T \Delta x^{2k+1} + C'_2 \Delta x^{k+2} \quad (3.20)$$

where C_1, C'_2 are positive constants independent of Δx . We only need to estimate the second part on the r.h.s. of (3.19). By Equation (2.11) and (3.17), after Taylor expansion, we have

$$\begin{aligned} \|\mathbf{u}_h(T) - \tilde{\mathbf{u}}_h(T)\| &\leq C \|\hat{\mathbf{u}}(T) - \tilde{\mathbf{u}}(T)\| \quad (3.21) \\ &\leq C \sum_{l=1}^{k+1} \left\| \exp(\lambda_l T) V_l - \sum_{l=1}^{k+1} \left(1 + \lambda_l \Delta t + \dots + \frac{\lambda_l^p \Delta t^p}{p!} \right)^{\frac{T}{\Delta t}} V_l \right\| \\ &\leq C \sum_{l=1}^{k+1} \left| \exp(\lambda_l T) - \left(1 + \lambda_l \Delta t + \dots + \frac{\lambda_l^p \Delta t^p}{p!} \right)^{\frac{T}{\Delta t}} \right| \|V_l\| \end{aligned}$$

- Firstly, we consider λ_1 .

$$\begin{aligned} &\left| \exp(\lambda_1 n \Delta t) - \left(1 + \Delta t \lambda_1 + \dots + \frac{\Delta t^p \lambda_1^p}{p!} \right)^n \right| \\ &\leq \left| \exp(\lambda_1 \Delta t) - \left(1 + \Delta t \lambda_1 + \dots + \frac{\Delta t^p \lambda_1^p}{p!} \right) \right| \\ &\quad \left| \sum_{m=0}^{n-1} \exp(\lambda_1 m \Delta t) \left(1 + \Delta t \lambda_1 + \dots + \frac{\Delta t^p \lambda_1^p}{p!} \right)^{n-1-m} \right| \\ &\leq C'_3 T \Delta t^p \quad (3.22) \end{aligned}$$

where the last inequality requires the estimate about λ_1 from Proposition. 3.1,

$$|\exp(\lambda_1 m \Delta t)| < 1, \quad \forall m.$$

We also need

$$\left|1 + \lambda_1 \Delta t + \dots + \frac{(\lambda_1 \Delta t)^p}{p!}\right|^m \leq C'_3, \quad \forall m \leq n-1 \quad (3.23)$$

To guarantee such inequality, the time step Δt has to be small enough for stability. Below, we only consider a simple case to illustrate how time step restriction is related to the stability, and the equation (3.23). The readers are referred to [12] for more details.

RKDG scheme with P^1 with RK2. Denote $cfl = \frac{\Delta t}{\Delta x}$ and $\xi = \omega \Delta x$. From Prop. 3.1, we have

$$\begin{aligned} \lambda_1 &= -i\omega - \frac{\omega^4}{72} \Delta x^3 - \frac{i\omega^5}{270} \Delta x^4 + O(\Delta x^5) \\ &= -i\omega - \frac{\xi^4}{72\Delta x} - \frac{i\xi^5}{270\Delta x} + O(\xi^5). \end{aligned}$$

Then

$$\begin{aligned} \left|1 + \lambda_1 \Delta t + \frac{\lambda_1^2 \Delta t^2}{2}\right|^2 &= \left|1 - icfl\xi - \frac{cfl^2}{2}\xi^2 - \frac{cfl}{72}\xi^4 + O(\xi^5)\right|^2 \\ &= \left|1 + \left(\frac{cfl^4}{4} - \frac{cfl}{36}\right)\xi^4 + O(\xi^6)\right|. \end{aligned}$$

We require the lead term

$$\frac{cfl^4}{4} - \frac{cfl}{36} < 0,$$

which leads to $cfl < 0.48075$. Note that this is necessary, but not sufficient condition to have (3.23) for all $\xi \in [0, 2\pi]$.

- For $\lambda_l, l \geq 2$. From Prop. 3.1, we have

$$\begin{aligned} \left| \exp(\lambda_l T) - \left(1 + \lambda_l \Delta t + \dots + \frac{\lambda_l^p \Delta t^p}{p!}\right)^{\frac{T}{\Delta t}} \right| &\leq \left| \exp(\lambda_l T) \right| + \left| \left(1 + \lambda_l \Delta t + \dots + \frac{\lambda_l^p \Delta t^p}{p!}\right)^{\frac{T}{\Delta t}} \right| \\ &\leq C_2^l, \end{aligned} \quad (3.24)$$

if

$$\left|1 + \lambda_l \Delta t + \dots + \frac{\lambda_l^p \Delta t^p}{p!}\right| \leq C'_2. \quad (3.25)$$

This inequality would be valid only for sufficiently small time step as for λ_1 . Below, we use the same example as above to derive a necessary condition for linear stability.

RKDG scheme with P^1 with RK2. From Proposition 3.1, we have

$$\lambda_2 = -\frac{6}{\Delta x} + \mathcal{O}(1),$$

then

$$\left|1 + \lambda_2 \Delta t + \frac{\lambda_2^2 \Delta t^2}{2}\right| \leq |1 - 6cfl + 18cfl^2| + \mathcal{O}(\xi)$$

To ensure stability, we need

$$|1 - 6cfl + 18cfl^2| < 1 \quad i.e. \quad cfl < \frac{1}{3}.$$

Combining the two time step restrictions, we get $cfl < \frac{1}{3}$, which is a necessary condition for linear stability of RKDG scheme with P^1 with RK2. Such time step restriction is consistent with the classical results in [10]. Similar analysis can be performed for general RKDG methods.

Now we can finish the proof. Under certain linear stability constrain of time step Δt , we have from the above discussions

$$\|\mathbf{u}_h(T) - \tilde{\mathbf{u}}_h(T)\| \leq C_3 T \Delta t^p + C \sum_l C_2^l \Delta x^{k+2} \quad (3.26)$$

where $C_3 = CC_3'$ is a positive constant independent of Δx and Δt . Combine (3.19), (3.20) and (3.26), we derive the final error estimate with $C_2 = C_2' + C \sum_l C_2^l$. ■

Remark 3.26. In the proof, we do not intend to derive a necessary and sufficient condition of the time step restriction. Related work on this topic can be found [15]. We only assume such time step restriction is satisfied for the linear stability, then the error estimate for the fully discretized scheme can be derived.

Similarly, an error estimate of fully discretized LDG scheme with p^{th} order explicit RK method can also be derived.

Proposition 3.27. With the same assumption as Proposition 3.20. Denote $\tilde{\mathbf{u}}_h$ as the numerical solution of fully discretized LDG scheme with k^{th} order polynomial as solutions space

and p^{th} order RK method and $\tilde{\mathbf{e}} = \mathbf{u} - \tilde{\mathbf{u}}_h$. Then for $T > 0$, and under certain linear stability constrain for time step Δt , we have the error estimate

$$\|\tilde{\mathbf{e}}(T)\| \leq C_1 T \Delta x^{2k+2} + C_2 \Delta x^{k+2} + C_3 T \Delta t^p, \quad (3.27)$$

where C_1, C_2, C_3 are positive constants independent of Δx and Δt . Here that $\|\cdot\|$ can be any norm for vectors.

Proof. The proof is similar to Proposition 3.25.

Remark 3.28. For a fully discretized RKDG scheme, the results in Remark 3.8 still hold, provided the order of RK method $p \geq 2k + 1$. If a low order of RK method is used with $\Delta t = \mathcal{O}(\Delta x)$, the error will grow linearly with time, see [24] for a detailed numerical comparison. In general, in order to study the superconvergence property of DG and LDG scheme, we use very high order RK method (SSPRK(9,9)) or let $\Delta t = \mathcal{O}(\Delta x^2)$ to reduce temporal errors.

4 Numerical examples

In this section, we provide a collection of one- and two-dimensional numerical experiments to verify our theoretical analysis in Section 3. DG schemes for a one-dimensional linear equation based on non-uniform mesh, one-dimensional nonlinear Burgers' equation, two-dimensional systems such as wave equations and Maxwell equations are also investigated to explore superconvergence properties of DG methods in a more general setting. We do not report DG errors at Radau points due to superconvergence properties of physically relevant eigenvectors in this paper, as they have been well documented in [26]. In our numerical experiments in this section, we use explicit p_1 -stage, p_2 -order strong stability preserving Runge-Kutta methods [11], denotes as SSPRK(p_1, p_2) for time discretization. In most of our simulations below, we use SSPRK(9,9) for linear problems and use SSPRK(5,4) for nonlinear problems. We also reduce the time step size so that the spatial error from DG is the dominant error. We use Gaussian quadrature rule with $k + 1$ quadrature points to compute the volume integral in the DG formulation, which is exact for linear cases and is of order $2k + 2$ for variable coefficient cases nonlinear cases. We use the same quadrature rule to compute the L^2 norm of error functions. We remark that since Gaussian quadrature rule

is of order $2k + 2$ for $k + 1$ Gauss points, $(2k + 1)^{th}$ order of convergence will be able to be maintained numerically.

Example 4.1. Consider a one-dimensional linear advection equation:

$$\begin{cases} u_t + u_x = 0, & x \in [0, 2\pi] \\ u(x, 0) = \sin(x) \end{cases} \quad (4.1)$$

with periodic boundary conditions. In order to make the temporal error negligible compared to the spatial error, we adopt SSPRK(9,9) [11] to solve $du/dt = Lu$, where L is DG discretization operator. Note that in order to use SSPRK(9,9), L should be a linear operator. In the simulation, we choose $CFL = 0.3$ for P^1 , $CFL = 0.2$ for P^2 and $CFL = 0.1$ for P^3 .

In this example, we consider two type of DG errors. One is the regular DG error ($e = u - u_h$), and the other is

$$\bar{e}_n = |u_h(T = 2\pi) - u_h(T = 2(n + 1)\pi)|, \quad n \in \mathbb{N}, \quad (4.2)$$

whose order of convergence is $2k + 1$ as discussed in Corollary 3.9. In Table 4.1 and 4.2 we report the L^2 norm of \bar{e}_1 and \bar{e}_2 , and the order of accuracy for P^1 - P^3 . $(2k + 1)^{th}$ order of accuracy is observed, as expected from Corollary 3.9. It is also observed that $\bar{e}_2 \approx 2\bar{e}_1$ indicating the linear growth rate of the error in time. This is also consistent with the Corollary 3.9. In Figure 4.1, the evolution of L^2 norms of the regular DG errors $e(t)$ and $\bar{e}_n(t)$ in a log-log scale is provided. The magnitude of regular DG error is observed to be much larger than \bar{e}_n . It is observed that the regular DG error does not grow for a long time, while linear growth rate of the error \bar{e}_n with respect to time is observed, see Remark 3.10. In Figure 4.2 - 4.4, we plot the regular errors of DG schemes and the errors \bar{e}_1 with $n = 1$ in equation (4.2) in a logarithmic scale for P^1 - P^3 . Highly oscillatory nature of DG errors are observed as in [9]. On the other hand, \bar{e}_1 does not oscillate as much; the magnitude of \bar{e}_1 is much smaller and the order is $2k + 1$.

A non-uniform mesh with two different mesh sizes is used to assess superconvergence properties of DG with non-uniform mesh. We set $\Delta x_{\text{left}}/\Delta x_{\text{right}} = 3/2$, where Δx_{left} and Δx_{right} is the mesh size for the left and right half part of the domain respectively. In Table 4.3, we report the error \bar{e}_1 . An order of $2k + 1$ is observed for P^1 and P^2 cases, but not for the P^3 case. We remark that in [26], with non-uniform mesh, $(2k + 1)^{th}$ order of convergence

is not observed well at downwind points for the case of P^3 either. Figure 4.5 shows error \bar{e}_1 in logarithmic scale for P^1 - P^3 when $N = 70$. Non-oscillatory errors are observed for P^1 and P^2 even around the interface of different mesh sizes. For P^3 , the error is observed to be oscillatory near the discontinuity of mesh size.

Table 4.1: Linear advection $u_t + u_x = 0$ with initial condition $u(x, 0) = \sin(x)$. The L^2 norm of \bar{e}_1 and the order of accuracy. Uniform mesh.

mesh	P^1		P^2		P^3	
	L^2 error	order	L^2 error	order	L^2 error	order
20	4.74E-03	–	4.71E-06	–	2.39E-09	–
30	1.41E-03	2.98	6.22E-07	4.99	1.39E-10	7.01
40	5.98E-04	2.99	1.48E-07	5.00	1.86E-11	7.00
50	3.06E-04	3.00	4.84E-08	5.00	3.90E-12	7.00
60	1.77E-04	3.00	1.95E-08	5.00	1.09E-12	7.00

Table 4.2: Linear advection $u_t + u_x = 0$ with initial condition $u(x, 0) = \sin(x)$. The L^2 norm of \bar{e}_2 and the order of accuracy. Uniform mesh.

mesh	P^1		P^2		P^3	
	L^2 error	order	L^2 error	order	L^2 error	order
20	9.47E-03	–	9.42E-06	–	4.76E-09	–
30	2.83E-03	2.98	1.24E-06	4.99	2.79E-10	7.00
40	1.20E-03	2.99	2.96E-07	5.00	3.72E-11	7.00
50	6.13E-04	3.00	9.69E-08	5.00	7.81E-12	7.00
60	3.55E-04	3.00	3.89E-08	5.00	2.18E-12	7.00

Example 4.2. Consider the same advection equation as Example 4.1 but with a different initial condition:

$$u(x, 0) = \exp(\sin(x)). \quad (4.3)$$

Note that the initial condition contains infinite number of Fourier modes. In Table 4.4, we report the L^2 norm of \bar{e}_1 and the order of accuracy. $(2k + 1)^{th}$ order of accuracy is observed as expected.

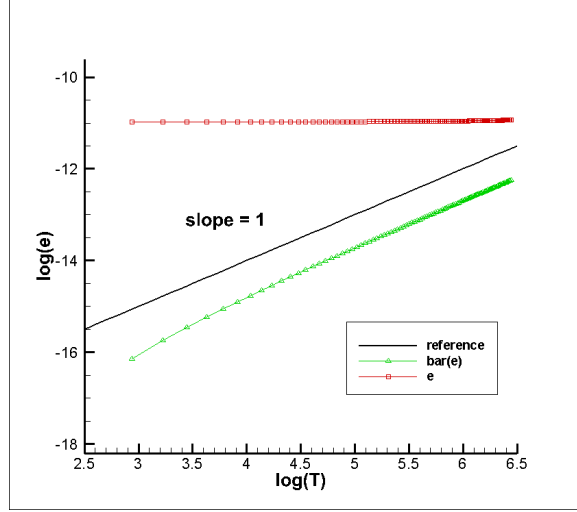


Figure 4.1: DG with P^2 , $u_t + u_x = 0$, the evolution of L^2 norms of regular DG error and error $|\bar{e}_n|$. A reference line with slope 1 is plotted as the reference of linear growth rate of $|\bar{e}_n|$ with respect to time. In the simulation, we use RKDG P^2 with mesh size $\Delta x = \frac{2\pi}{50}$ and $CFL = 0.2$.

Example 4.3. Consider the following linear variable coefficient equation:

$$\begin{cases} u_t + (a(x)u)_x = b(x, t), & x \in [0, 2\pi] \\ u(x, 0) = \sin(x) \end{cases} \quad (4.4)$$

with periodic boundary conditions. And $a(x)$ and $b(x, t)$ are given by

$$a(x) = \sin(x) + 2, \quad b(x, t) = (\sin(x) + 3) \cos(x + t) + \cos(x) \sin(x + t). \quad (4.5)$$

The exact solution is $u(x, t) = \sin(x+t)$. We use SSPRK(5,4) for the temporal discretization. In the simulation, we let $CFL = \frac{1}{3}$ for P^1 , $CFL = \frac{1}{5}$ for P^2 and $CFL = \frac{1}{7}$ for P^3 , and time step $\Delta t = CFL\Delta x^2$ to reduce the time errors. We report the L^2 norm of \bar{e}_1 as defined in equation (4.2) and numerical order of accuracy in Table 4.5. $(2k + 1)^{th}$ order of accuracy is observed, although our analysis only works for the constant coefficient problems.

Example 4.4. Consider the following nonlinear Burgers' equation with a source term:

$$\begin{cases} u_t + (u^2)_x = b(x, t) & x \in [0, 2\pi] \\ u(x, 0) = \sin(x) + c \end{cases} \quad (4.6)$$

with periodic boundary conditions. Here c is a real number and $b(x, t)$ is given by

$$b(x, t) = \cos(x + t)(2c + 1 + 2 \sin(x + t)). \quad (4.7)$$

Table 4.3: Linear advection $u_t + u_x = 0$ with initial condition $u(x, 0) = \sin(x)$. The L^2 norm of \bar{e}_1 and the order of accuracy. Nonuniform mesh with two different mesh sizes. $\Delta x_{\text{left}}/\Delta x_{\text{right}} = 3/2$.

	P^1		P^2		P^3	
mesh	L^2 error	order	L^2 error	order	L^2 error	order
20	3.37E-03	–	5.61E-06	–	2.45E-08	–
30	1.01E-03	2.98	7.42E-07	4.99	1.49E-09	6.90
40	4.27E-04	2.99	1.76E-07	5.00	2.32E-10	6.46
50	2.19E-04	2.99	5.78E-08	5.00	6.00E-11	6.07
60	1.27E-04	3.00	2.32E-08	5.00	2.03E-11	5.93
70	7.98E-05	3.00	1.07E-08	5.00	2.03E-11	5.95

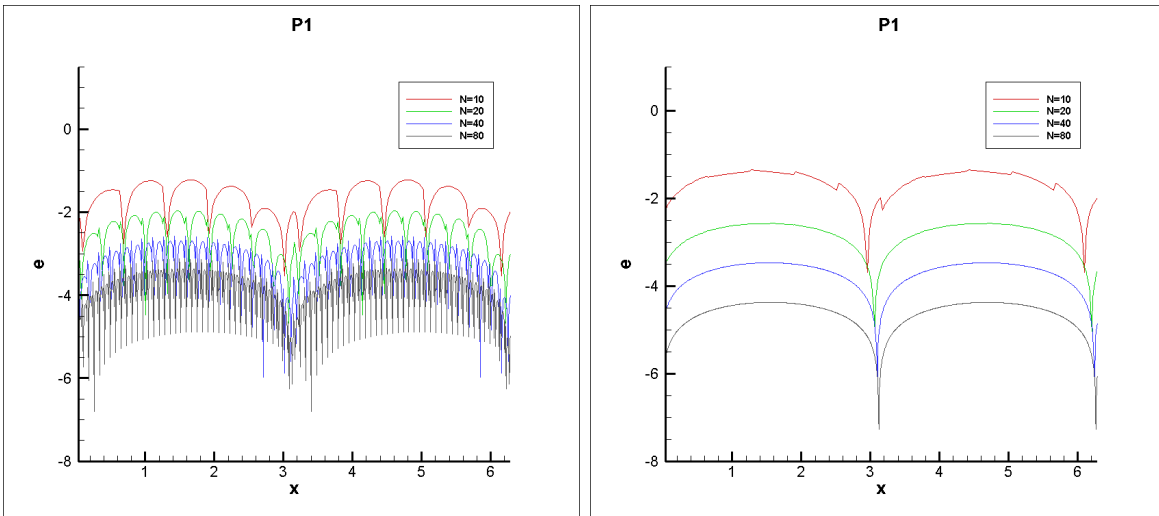


Figure 4.2: DG with P^1 , $u_t + u_x = 0$, regular error $|u(T = 4\pi) - u_h(T = 4\pi)|$ (left); error $|\bar{e}_1|$ (right).

The exact solution is $u(x, t) = \sin(x+t) + c$. We use SSPRK(5,4) for the temporal discretization. In the simulation, we let $CFL = \frac{1}{3}$ for P^1 , $CFL = \frac{1}{5}$ for P^2 and $CFL = \frac{1}{7}$ for P^3 , and time step $\Delta t = CFL\Delta x^2$ to reduce the time errors. Firstly, we let $c = 0$, and compute the error \bar{e}_1 . In Table 4.6, the L^2 error and the order of accuracy are reported. $(2k + 1)^{th}$ order of accuracy is not observed. Note that the wave speed is $2u$, and there exist some regions around which wave travels at very slow speed (i.e. the region around which $u = 0$). In these regions, the non physically relevant eigenvectors are damped very slowly with time, see the second term on the r.h.s. of equation (3.3), see also Remark 3.11. $(2k + 1)^{th}$ order is not observed numerically. In Figure 4.6, \bar{e}_1 in logarithmic scale for $P^1 - P^3$ cases are plotted

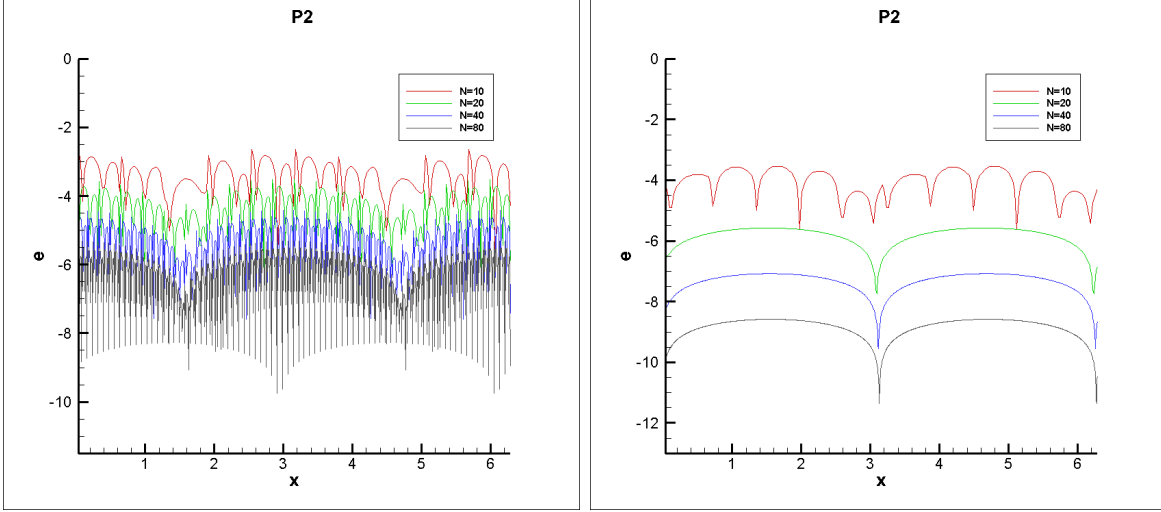


Figure 4.3: DG with P^2 , $u_t + u_x = 0$, regular error $|u(T = 4\pi) - u_h(T = 4\pi)|$ (left); error $|\bar{e}_1|$ (right).

Table 4.4: Linear advection $u_t + u_x = 0$ with initial condition $u(x, 0) = \exp(\sin(x))$. The L^2 norm of \bar{e}_1 and the order of accuracy. Uniform mesh.

mesh	P^1		P^2		P^3	
	L^2 error	order	L^2 error	order	L^2 error	order
30	7.80E-03	–	2.68E-05	–	7.08E-08	–
40	3.42E-03	2.86	6.41E-06	4.96	9.54E-09	6.97
50	1.78E-03	2.93	2.11E-06	4.98	2.01E-09	6.98
60	1.04E-03	2.96	8.51E-07	4.99	5.62E-10	6.99
70	6.57E-04	2.97	3.94E-07	4.99	1.91E-10	6.99

when $N = 100$. It is observed that \bar{e}_1 dominates around $x = \pi$. Then, we set $c = 2$. In this case, there is a positive lower bound on the wave speed. We report the L^2 norm of \bar{e}_1 and numerical order of accuracy in Table 4.7. The $(2k + 1)^{th}$ order is observed. In Figure 4.7 - 4.9, we plot the regular errors of DG schemes and \bar{e}_1 in logarithmic scale for $P^1 - P^3$ cases. While highly oscillatory nature of regular errors is observed, \bar{e}_1 is observed to be much less oscillatory with much smaller magnitude. We remark that although for the $c = 0$ case, $(2k + 1)^{th}$ order of accuracy can't be observed numerically, the long time behavior of the error as commented in Remark 3.8 still holds.

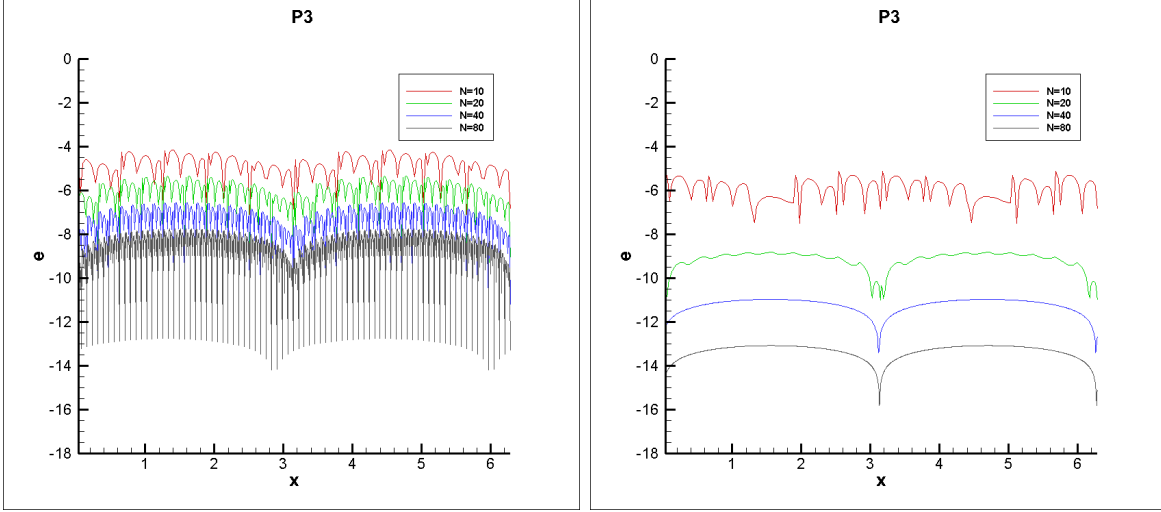


Figure 4.4: DG with P^3 , $u_t + u_x = 0$, regular error $|u(T = 4\pi) - u_h(T = 4\pi)|$ (left); error $|\bar{e}_1|$ (right).

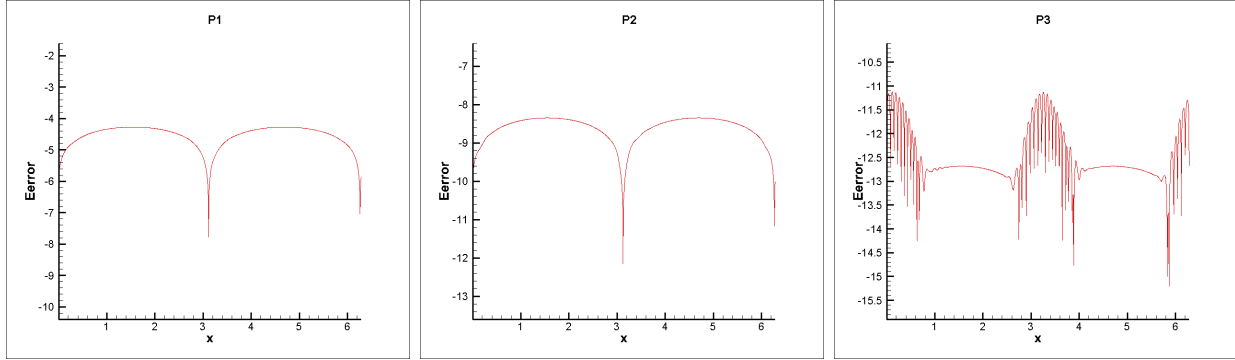


Figure 4.5: DG scheme for $u_t + u_x = 0$, error $|\bar{e}_1|$, nonuniform mesh with two different mesh sizes, $\Delta x_{\text{left}}/\Delta x_{\text{right}} = 3/2$, $N = 70$, P^1 (left), P^2 (middle), P^3 (right).

Example 4.5. We consider the following one-dimensional system:

$$\begin{cases} \begin{pmatrix} u \\ v \end{pmatrix}_t + \begin{pmatrix} 0 & 1 \\ 1 & 0 \end{pmatrix} \begin{pmatrix} u \\ v \end{pmatrix}_x = \begin{pmatrix} 0 \\ 0 \end{pmatrix} \\ u(x, 0) = \sin x \\ v(x, 0) = \cos x \end{cases} \quad (4.8)$$

with periodic boundary conditions. Note that this is a one-dimensional wave equation written as a first order hyperbolic linear system. The upwind flux is used for DG scheme and SSPRK(9,9) is used for temporal discretization in the simulation. We let $CFL = \frac{1}{3}$ for P^1 , $CFL = \frac{1}{5}$ for P^2 and $CFL = \frac{1}{7}$ for P^3 . We report the L^2 norm of \bar{e}_1 and the order of accuracy for the u variable in Table 4.8. $(2k + 1)^{\text{th}}$ order is observed.

Table 4.5: Linear variable coefficient problem. The L^2 norm of \bar{e}_1 and the order of accuracy. Uniform mesh.

	P^1		P^2		P^3	
mesh	L^2 error	order	L^2 error	order	L^2 error	order
20	5.00E-04	–	9.43E-07	–	8.70E-08	–
30	1.68E-04	2.68	1.24E-07	5.00	5.66E-09	6.74
40	7.37E-05	2.87	2.95E-08	5.00	7.42E-10	7.06
50	3.83E-05	2.93	9.67E-09	5.00	1.20E-10	8.17
60	2.23E-05	2.96	3.88E-09	5.00	2.26E-11	9.15

Table 4.6: Nonlinear Burgers' equation: $u_t + (u^2)_x = b(x, t)$ with initial condition $u(x, 0) = \sin(x)$. The L^2 norm of \bar{e}_1 measured from solutions at Gaussian points of each cell and the order of accuracy. Uniform mesh.

	P^1		P^2		P^3	
mesh	L^2 error	order	L^2 error	order	L^2 error	order
50	1.30E-07	–	8.34E-09	–	1.93E-10	–
60	9.21E-08	1.91	3.96E-09	4.08	1.10E-10	3.09
70	6.79E-08	1.98	1.85E-09	4.95	5.95E-11	3.98
80	5.23E-08	1.95	1.13E-09	3.69	4.00E-11	2.97
90	4.18E-08	1.90	4.76E-10	7.34	2.75E-11	3.19
100	3.43E-08	1.88	3.29E-10	3.48	1.80E-11	4.00

Example 4.6. We consider the following one-dimensional diffusion equation:

$$\begin{cases} u_t = u_{xx}, & x \in [0, 2\pi] \\ u(x, 0) = \sin(x) \end{cases} \quad (4.9)$$

with periodic boundary conditions. The exact solution of (4.9) is

$$u(x, t) = \exp(-t) \sin x.$$

We use a LDG method with SSPRK(9,9) temporal discretization to solve the equation. In the simulation, we use $CFL = 0.01$ and $\Delta t = CFL\Delta x^2$. We let u_h denote the numerical solution for u and p_h denote that for u_x . We compare the the error

$$\tilde{e}_1 = \exp(-1)u_h(T = 1) - u_h(T = 2), \quad (4.10)$$

and

$$\tilde{e}_2 = \exp(-1)p_h(T = 1) - p_h(T = 2). \quad (4.11)$$

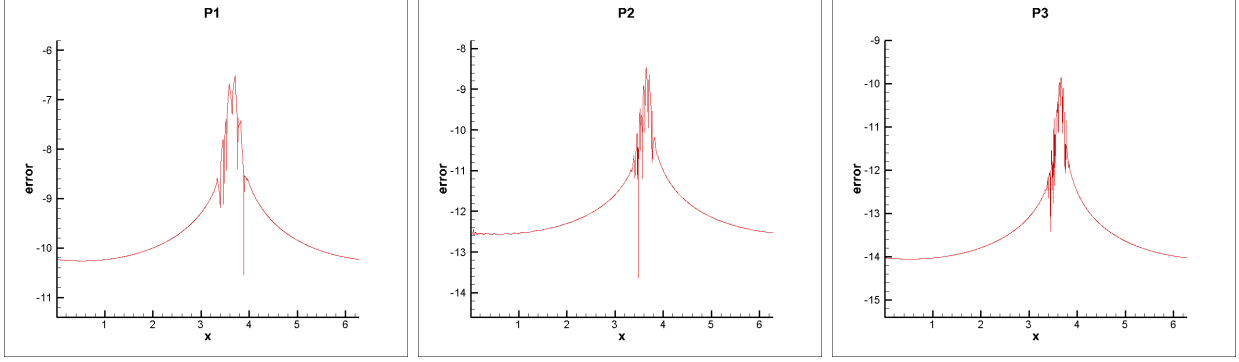


Figure 4.6: DG scheme for nonlinear Burgers' equation with initial condition $u(x, 0) = \sin(x)$, error \bar{e}_1 , $N = 100$, P^1 (left), P^2 (middle), P^3 (right).

Table 4.7: Nonlinear Burgers' equation: $u_t + (u^2)_x = b(x, t)$ with initial condition $u(x, 0) = \sin(x) + 2$. The L^2 norm of \bar{e}_1 measured from solutions at Gaussian points of each cell and the order of accuracy. Uniform mesh.

	P^1		P^2		P^3	
mesh	L^2 error	order	L^2 error	order	L^2 error	order
50	3.64E-05	–	6.61E-09	–	1.76E-12	–
60	2.11E-05	2.98	2.66E-09	5.00	2.53E-13	10.64
70	1.33E-05	2.99	1.23E-09	5.00	7.45E-14	7.92
80	8.93E-06	2.99	6.30E-10	5.00	2.88E-14	7.12
90	6.27E-06	2.99	3.50E-10	5.00	1.26E-14	7.03
100	4.57E-06	3.00	2.06E-10	5.00	6.01E-15	7.02

In Table 4.9 and Table 4.10, we report the L^2 norm of \tilde{e}_1 and \tilde{e}_2 . $(2k+2)^{th}$ order of accuracy is observed as expected from Corollary 3.23. In Figure 4.10 - 4.12, we plot the regular errors of LDG schemes and the errors \tilde{e}_1 in logarithmic scale for P^1 - P^3 . Regular errors are observed to be highly oscillatory, while \tilde{e}_1 is much less oscillatory with much smaller magnitude.

Example 4.7. We consider the following two-dimensional advection equation:

$$\begin{cases} u_t + u_x + u_y = 0, & (x, y) \in [0, 2\pi] \times [0, 2\pi] \\ u(x, y, 0) = \sin(x + y) \end{cases} \quad (4.12)$$

with periodic boundary conditions in both x and y directions. The exact solution of (4.12) is

$$u(x, y, t) = \sin(x + y - 2t).$$

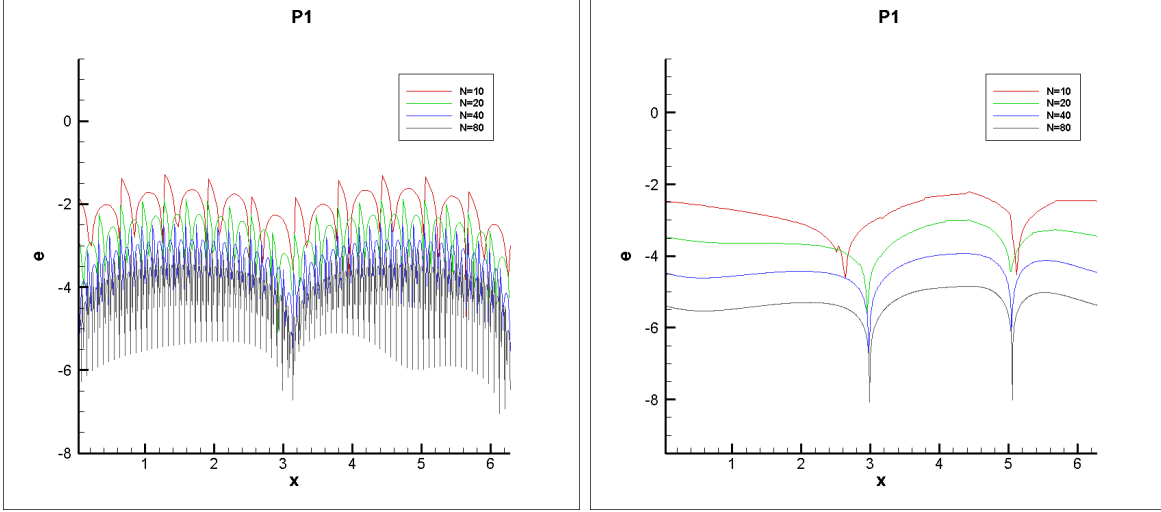


Figure 4.7: DG with P^1 ; nonlinear Burgers' equation with initial condition $u(x, 0) = \sin(x) + 2$; regular error $|u(T = 4\pi) - u_h(T = 4\pi)|$ (left); $|\bar{e}_1|$ (right).

Table 4.8: The linear system (4.8). The L^2 norm of \bar{e}_1 and the order of accuracy for variable u . Uniform mesh.

	P^1		P^2		P^3	
mesh	L^2 error	order	L^2 error	order	L^2 error	order
30	6.52E-04	–	3.38E-07	–	8.58E-11	–
40	2.80E-04	2.94	8.11E-08	4.86	1.15E-11	6.99
50	1.45E-04	2.96	2.67E-08	4.97	2.42E-12	6.98
60	8.43E-05	2.97	1.08E-08	4.98	6.78E-13	6.98
70	5.33E-05	2.97	5.00E-09	4.98	2.31E-13	6.99

Firstly, we use DG with the Q^k space, see equation (3.5). We compute the error

$$\bar{e}_1 = u_h(T = \pi) - u_h(T = 2\pi). \quad (4.13)$$

In Table 4.11, we report the L^2 norm of \bar{e}_1 and the order of accuracy. $(2k + 1)^{th}$ order of accuracy is observed. In the simulations for 2-D cases, the time step is chosen as

$$\Delta t = CFL \left(\frac{\Delta x}{c_1} + \frac{\Delta y}{c_2} \right),$$

where c_x and c_y are maximum wave propagation speed in x -direction and y -direction respectively. We choose $CFL = 0.1$. Then, we use DG with the P^k space, see equation (3.10). We give the L^2 norm of \bar{e}_1 and the order of accuracy in Table 4.12. Again $(2k + 1)^{th}$ order

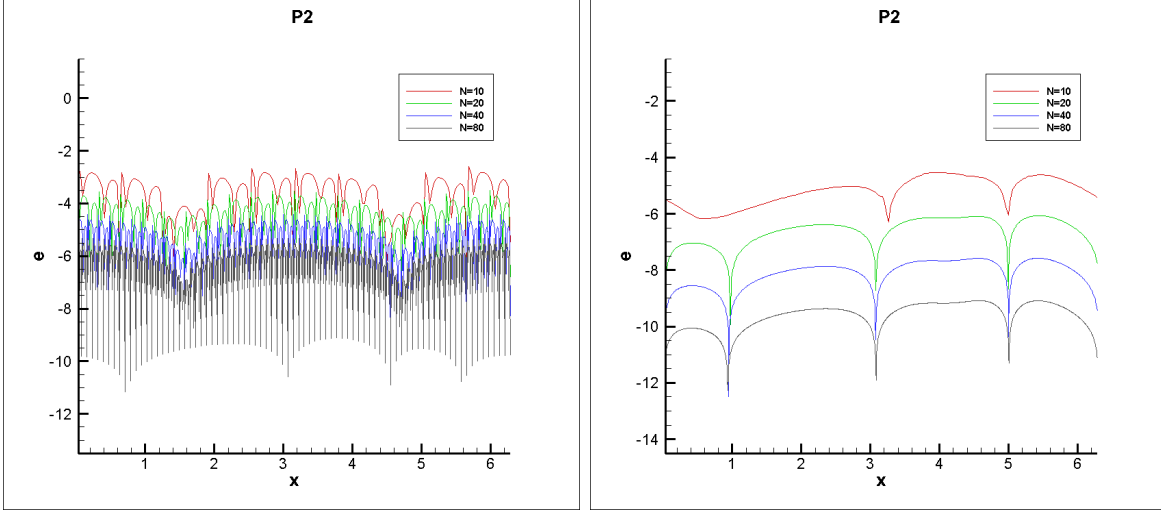


Figure 4.8: DG with P^2 ; nonlinear Burgers' equation with initial condition $u(x, 0) = \sin(x) + 2$, regular error $|u(T = 4\pi) - u_h(T = 4\pi)|$ (left); $|\bar{e}_1|$ (right).

Table 4.9: Diffusive equation $u_t = u_{xx}$. The L^2 norm and order of accuracy of \tilde{e}_1 . Uniform mesh.

	P^1		P^2		P^3	
mesh	L^2 error	order	L^2 error	order	L^2 error	order
10	3.99E-05	–	8.15E-08	–	1.04E-10	–
20	2.45E-06	4.02	1.27E-09	6.01	4.08E-13	8.00
30	4.83E-07	4.01	1.11E-10	6.00	1.59E-14	8.00
40	1.53E-07	4.00	1.98E-11	6.00	1.60E-15	8.00
50	6.26E-08	4.00	5.18E-12	6.00	2.68E-16	8.00

of accuracy is observed. The magnitude of error appears to be larger than those from DG scheme with a Q^k space. In Figure 4.13, the DG error in 3-D and contour plot are reported.

Example 4.8. We consider the rigid body rotation problem:

$$u_t - yu_x + xu_y = 0, \quad (x, y) \in [-\pi, \pi] \times [-\pi, \pi], \quad (4.14)$$

with the following smooth initial condition:

$$u(x, y, 0) = \begin{cases} \cos^{12}(r) & r < \frac{\pi}{2}, \\ 0 & \text{otherwise,} \end{cases} \quad (4.15)$$

where $r = \sqrt{(x - \pi/2)^2 + y^2}$. As before, we calculate the error

$$\bar{e}_1 = u_h(T = 2\pi) - u_h(T = 4\pi).$$

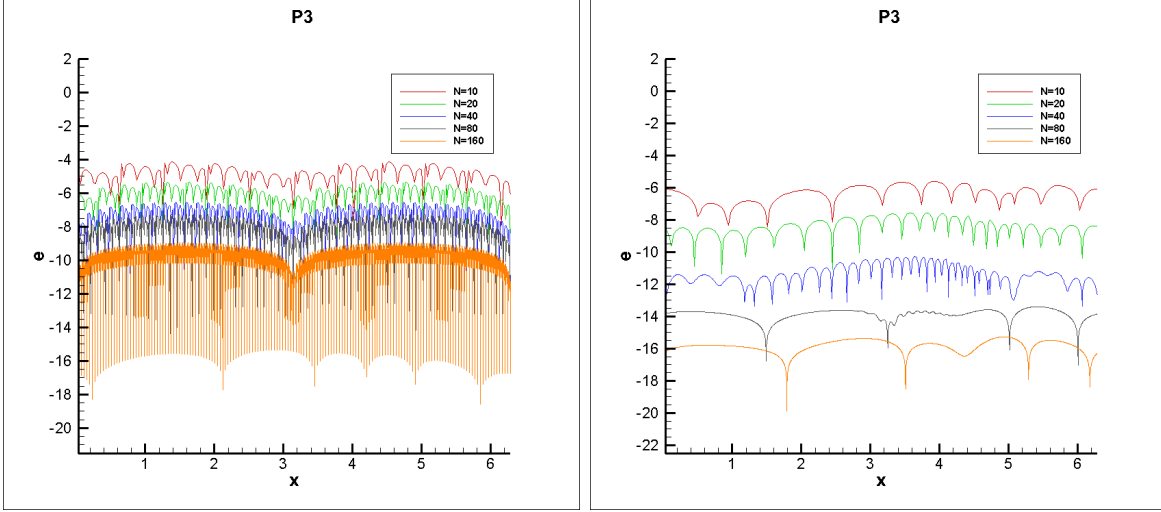


Figure 4.9: DG with P^3 ; nonlinear Burgers' equation with initial condition $u(x, 0) = \sin(x) + 2$; regular error $|u(T = 4\pi) - u_h(T = 4\pi)|$ (left); $|\bar{e}_1|$ (right).

Table 4.10: Diffusive equation $u_t = u_{xx}$. The L^2 norm of \tilde{e}_2 and the order of accuracy. Uniform mesh.

	P^1		P^2		P^3	
mesh	L^2 error	order	L^2 error	order	L^2 error	order
10	4.08E-05	–	8.15E-08	–	1.04E-10	–
20	2.47E-06	4.05	1.27E-09	6.01	4.08E-13	8.00
30	4.85E-07	4.01	1.11E-10	6.00	1.59E-14	8.00
40	1.53E-07	4.01	1.98E-11	6.00	1.60E-15	8.00
50	6.26E-08	4.00	5.18E-12	6.00	2.68E-16	8.00

In the simulation, we adopt the approximation space P^k for spatial discretization and SSPRK(5,4) for temporal discretization. We choose $CFL = 0.1$. In Table 4.13, we report L^2 norm of \bar{e}_1 and the order of accuracy. $(2k + 1)^{th}$ order is observed. Note that the mesh has to be fine enough to resolve the ‘cosine bell’ in order to observe a clean order of accuracy. Also note that the ‘cosine bell’ is centered at $(\pi/2, 0)$, which is away from the origin. Around the origin, the propagation speed $(-y, x)$ is close to zero. In such situation, the second term on the r.h.s. of Corollary 3.3 might dominate and $(2k + 1)^{th}$ order can't be observed. We omit to present the results to save space. Again, we remark that the long time behavior of the error as commented in Remark 3.8 still holds if the ‘cosine bell’ is positioned around the origin.

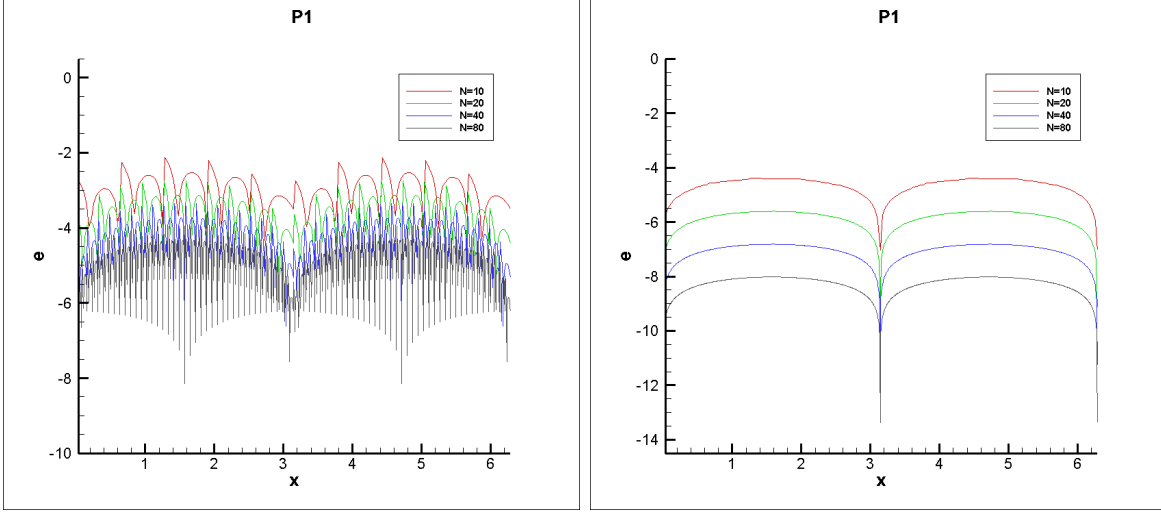


Figure 4.10: LDG with P^1 ; diffusive equation; regular error $|u(T = 2) - u_h(T = 2)|$ (left); $|\tilde{e}_1|$ (right)

Table 4.11: Two-dimensional advection equation $u_t + u_x + u_y = 0$. Q^k is used. The L^2 norm of \bar{e}_1 and the order of accuracy. Uniform mesh.

mesh	Q^1		Q^2		Q^3	
	L^2 error	order	L^2 error	order	L^2 error	order
30×30	3.55E-03	–	1.56E-06	–	4.62E-10	–
40×40	1.50E-03	2.99	3.70E-07	5.00	4.75E-11	7.90
50×50	7.68E-04	3.00	1.21E-07	5.00	9.79E-12	7.08
60×60	4.45E-04	3.00	4.88E-08	5.00	2.73E-12	7.00
70×70	2.80E-04	3.00	2.26E-08	5.00	9.28E-13	7.01

Example 4.9. We consider the following two-dimensional linear system:

$$\begin{cases} \begin{pmatrix} u \\ v \end{pmatrix}_t + \begin{pmatrix} -1 & 0 \\ 0 & 1 \end{pmatrix} \begin{pmatrix} u \\ v \end{pmatrix}_x + \begin{pmatrix} 0 & -1 \\ -1 & 0 \end{pmatrix} \begin{pmatrix} u \\ v \end{pmatrix}_y = \begin{pmatrix} 0 \\ 0 \end{pmatrix} \\ u(x, y, 0) = \frac{1}{2\sqrt{2}} \sin(x + y) - \frac{1}{2\sqrt{2}} \cos(x + y) \\ v(x, y, 0) = \frac{\sqrt{2}-1}{2\sqrt{2}} \sin(x + y) + \frac{\sqrt{2}+1}{2\sqrt{2}} \cos(x + y) \end{cases} \quad (4.16)$$

with periodic boundary conditions in both x and y directions. This is the second order wave equation written as a first order linear hyperbolic system and the exact solution is

$$\begin{cases} u(x, y, t) = \frac{1}{2\sqrt{2}} \sin(x + y + \sqrt{2}t) - \frac{1}{2\sqrt{2}} \cos(x + y - \sqrt{2}t) \\ v(x, y, t) = \frac{\sqrt{2}-1}{2\sqrt{2}} \sin(x + y + \sqrt{2}t) + \frac{\sqrt{2}+1}{2\sqrt{2}} \cos(x + y - \sqrt{2}t) \end{cases} \quad (4.17)$$

We remark that the two matrices in equation (4.16) don't commute, therefore the linear

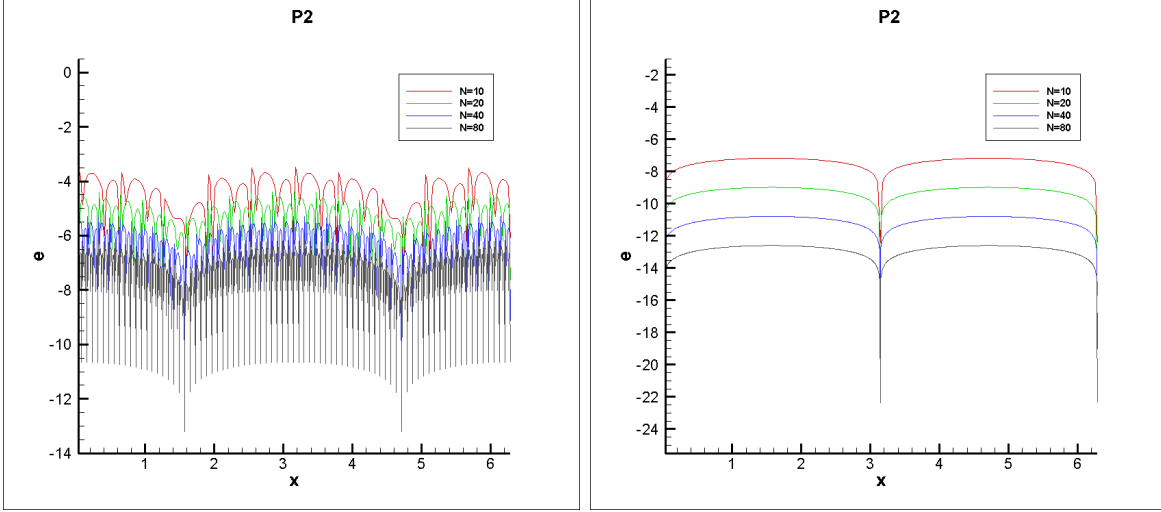


Figure 4.11: LDG with P^2 ; diffusive equation; regular error $|u(T = 2) - u_h(T = 2)|$ (left); $|\bar{e}_1|$ (right)

Table 4.12: Two-dimensional advection equation $u_t + u_x + u_y = 0$. P^k is used. The L^2 norm of \bar{e}_1 and the order of accuracy. Uniform mesh.

mesh	P^1		P^2		P^3	
	L^2 error	order	L^2 error	order	L^2 error	order
30×30	1.40E-02	–	2.22E-05	–	1.71E-08	–
40×40	5.96E-03	2.97	5.29E-06	4.99	2.28E-09	7.01
50×50	3.06E-03	2.98	1.74E-06	4.99	4.77E-10	7.00
60×60	1.77E-03	2.99	6.98E-07	5.00	1.33E-10	7.00
70×70	1.12E-03	2.99	3.23E-07	5.00	4.52E-11	7.01

system can't be reduced to 2-D scalar problems. In the simulation, the upwind flux and a SSPRK(9,9) scheme is used. We choose $CFL = 0.1$. Note that the period of the solution in time is $\sqrt{2}\pi$, that is $u(x, y, t) = u(x, y, t + \sqrt{2}\pi)$, then we let

$$\bar{e}_1 = u_h(T = 2) - u_h(T = 2 + \sqrt{2}\pi). \quad (4.18)$$

In Table 4.14, we report L^2 norm of \bar{e}_1 and the order of accuracy. $(2k + 1)^{th}$ order is observed. The error about the v variable is not presented to save space since it gives almost the same results.

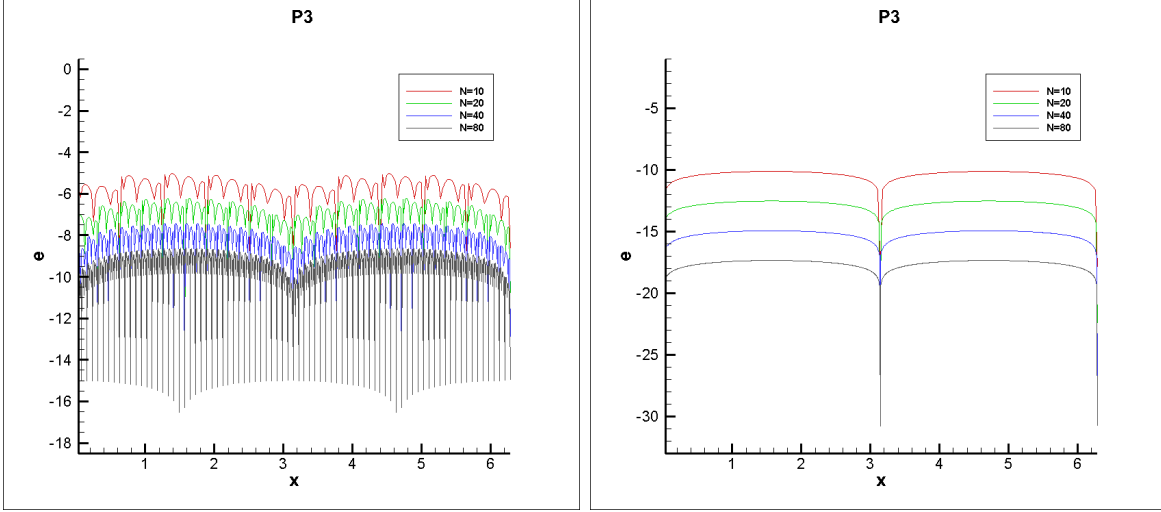


Figure 4.12: LDG with P^3 ; diffusive equation; regular error $|u(T = 2) - u_h(T = 2)|$ (left); $|\tilde{e}_1|$ (right)

Table 4.13: Rigid body rotation: $u_t - yu_x + xu_y = 0$. P^k is used. The L^2 norm of \bar{e}_1 and the order of accuracy. Uniform mesh.

mesh	P^1		P^2		P^3	
	L^2 error	order	L^2 error	order	L^2 error	order
100×100	9.98E-03	–	3.77E-05	–	9.33E-08	–
120×120	6.22E-03	2.59	1.53E-05	4.95	2.62E-08	6.97
140×140	4.09E-03	2.72	7.11E-06	4.97	8.94E-09	6.97
160×160	2.81E-03	2.81	3.66E-06	4.98	3.52E-09	6.98
180×180	2.01E-03	2.86	2.04E-06	4.98	1.55E-09	6.99
200×200	1.48E-03	2.89	1.20E-06	4.99	7.40E-10	6.99

Example 4.10. We consider the two-dimensional Maxwell equations:

$$\begin{cases} \frac{\partial H_x}{\partial t} + \frac{\partial E_z}{\partial y} = 0, \\ \frac{\partial H_y}{\partial t} - \frac{\partial E_z}{\partial x} = 0, \\ \frac{\partial E_z}{\partial t} - \frac{\partial H_y}{\partial x} + \frac{\partial H_x}{\partial y} = 0. \end{cases} \quad (4.19)$$

Note that the Maxwell equations are linear hyperbolic systems, which can be written as

$$U_t + AU_x + BU_y = 0, \quad (4.20)$$

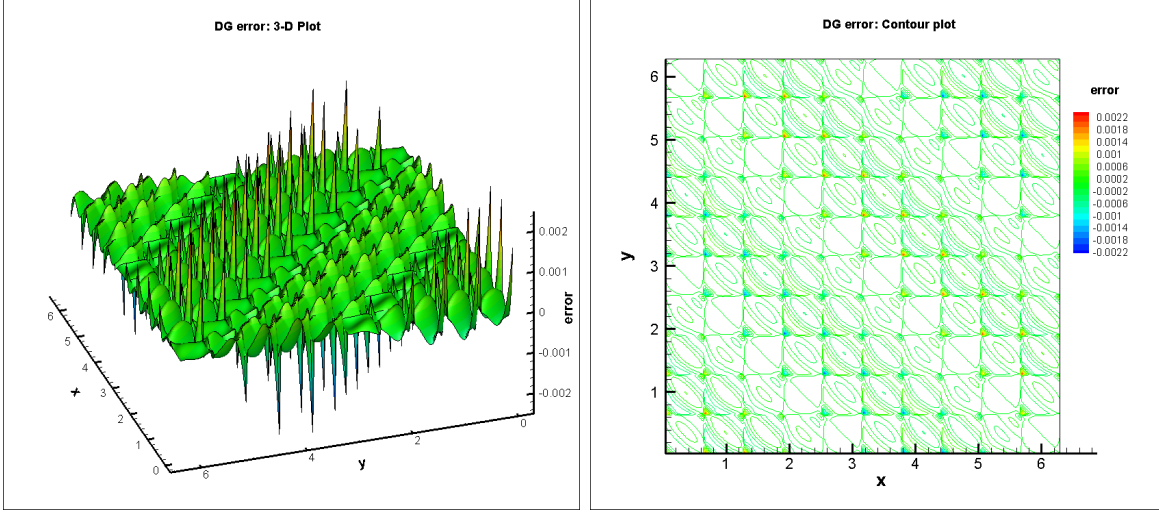


Figure 4.13: DG with P^3 ; 2-D linear advection equation $u_t + u_x + u_y = 0$; $N_x \times N_y = 10 \times 10$; 3-D plot of error $e = u(T = 4\pi) - u_h(T = 4\pi)$ (left); Contour of error $e = u(T = 4\pi) - u_h(T = 4\pi)$ (right)

Table 4.14: Two-dimensional linear system (4.16). P^k is used. The L^2 norm of \bar{e}_1 and the order of accuracy. Uniform mesh.

mesh	P^1		P^2		P^3	
	L^2 error	order	L^2 error	order	L^2 error	order
30×30	1.26E-02	–	1.40E-05	–	2.09E-08	–
40×40	5.34E-03	2.97	3.33E-06	4.99	2.51E-09	7.37
50×50	2.74E-03	2.99	1.09E-06	4.99	4.31E-10	7.91
60×60	1.59E-03	2.99	4.40E-07	4.99	1.14E-10	7.27
70×70	1.00E-03	3.00	2.04E-07	5.00	3.80E-11	7.14

where

$$A = \begin{pmatrix} 0 & 0 & 0 \\ 0 & 0 & -1 \\ 0 & -1 & 0 \end{pmatrix}, \quad B = \begin{pmatrix} 0 & 0 & 1 \\ 0 & 0 & 0 \\ 1 & 0 & 0 \end{pmatrix}. \quad (4.21)$$

For any unit vector $\mathbf{n} = (n_1, n_2)$, let

$$D = n_1 A + n_2 B. \quad (4.22)$$

Note that D always has three eigenvalues 1, -1 and 0 given a unit vector \mathbf{n} . It is easy to check that

$$\begin{cases} H_x = -\beta \cos(\alpha x + \beta y + t) \\ H_y = \alpha \cos(\alpha x + \beta y + t) \\ E_z = \cos(\alpha x + \beta y + t) \end{cases} \quad (4.23)$$

is an exact solution of Maxwell equations for $(x, y) \in [0, 2\pi/\alpha] \times [0, 2\pi/\beta]$, where $\alpha^2 + \beta^2 = 1$. This example is motivated by the work in [8], where the DG error after applying a post-processing technique are enhanced from $(k+1)^{th}$ order to $(2k+1)^{th}$ order. In the simulation, we take $\alpha = \beta = \frac{\sqrt{2}}{2}$. The upwind flux and a SSPRK(9,9) scheme is used. We choose $CFL = 0.1$. Let

$$\begin{aligned}\bar{e}_1 &= (E_z)_h(T = 4\pi) - (E_z)_h(T = 2\pi), \\ \bar{e}_2 &= (H_x)_h(T = 4\pi) - (H_x)_h(T = 2\pi), \\ \bar{e}_3 &= (H_y)_h(T = 4\pi) - (H_y)_h(T = 2\pi).\end{aligned}$$

In Table 4.15, we report L^2 norm of \bar{e}_1 and the orders of accuracy. The $(2k+1)^{th}$ order of accuracy is numerically observed for the P^1 and P^2 cases, but not for the P^3 case. In Table 4.16, we report L^2 norm of \bar{e}_2 and the orders of accuracy. $(2k+1)^{th}$ order of accuracy is not observed for the P^2 and P^3 cases. The reason we suspect is that there is one zero eigenvalue in D , along which the non physically relevant eigenvectors are not damped. In Figure 4.14, contours of \bar{e}_2 and \bar{e}_3 are plotted, for the DG with P^3 space. It is clear that \bar{e}_2 oscillates only in the x-direction and \bar{e}_3 oscillates only in the y-direction. Such observation suggests that the non-physically relevant eigenvectors of $(H_x)_h$ (or $(H_y)_h$) do not damp in x - (or y -) direction properly. We remark that although $(2k+1)^{th}$ order can't be observed for \bar{e}_2 and \bar{e}_3 . The DG solution can still be post processed to obtain $(2k+1)^{th}$ order as in [8]. The long time behavior of the magnitude of error as commented in Remark 3.8 might still hold.

Table 4.15: Two-dimensional Maxwell equations. P^k is used. The L^2 norm and order of accuracy of \bar{e}_1 of E_z . Uniform mesh.

mesh	P^1		P^2		P^3	
	L^2 error	order	L^2 error	order	L^2 error	order
20×20	6.82E-02	–	2.49E-04	–	5.49E-07	–
30×30	2.09E-02	2.92	3.34E-05	4.96	4.92E-08	5.95
40×40	8.91E-03	2.96	7.97E-06	4.98	9.65E-09	5.66
50×50	4.58E-03	2.98	2.62E-06	4.98	2.75E-09	5.62
60×60	2.66E-03	2.99	1.06E-06	4.99	9.84E-10	5.65

Table 4.16: Two-dimensional Maxwell equations. P^k is used. The L^2 norm and order of accuracy of \bar{e}_2 of H_x . Uniform mesh.

mesh	P^1		P^2		P^3	
	L^2 error	order	L^2 error	order	L^2 error	order
20×20	4.88E-02	–	4.00E-04	–	1.02E-05	–
30×30	1.51E-02	2.89	1.08E-04	3.23	1.97E-06	4.06
40×40	6.54E-03	2.92	4.12E-05	3.35	5.69E-07	4.32
50×50	3.40E-03	2.93	1.90E-05	3.47	2.10E-07	4.47
60×60	1.99E-03	2.94	9.93E-06	3.56	9.12E-08	4.57

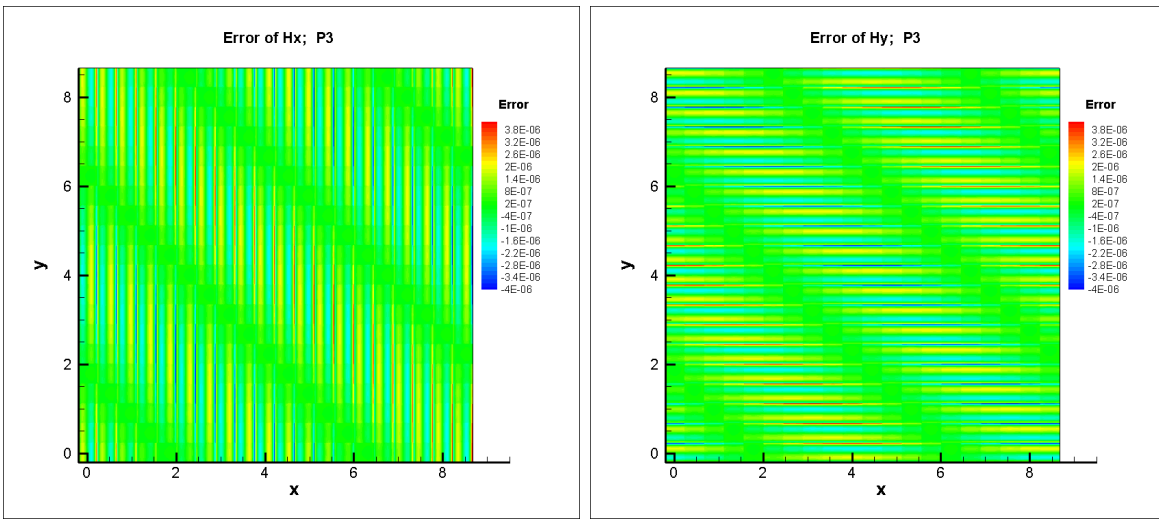


Figure 4.14: DG with P^3 for Maxwell equations; Contour of error $\bar{e}_2 = (H_x)_h(T = 4\pi) - (H_x)_h(T = 2\pi)$ (left); Contour of error $\bar{e}_3 = (H_y)_h(T = 4\pi) - (H_y)_h(T = 2\pi)$ (right)

5 Conclusion

In this paper, we discussed the superconvergence properties of discontinuous Galerkin (DG) and local DG (LDG) methods for linear hyperbolic and parabolic problems via Fourier approach. Especially, superconvergence properties of DG with uniform mesh for linear problems with periodic boundary conditions are discussed in terms of

- dissipation and dispersion error of physically relevant eigenvalues; this part of error is related to the negative norm of DG error as discussed in [9, 16]
- eigenvectors with Lagrangian basis functions based on shifted Radau-points; this part of error is related to superconvergence at Radau points as discussed in [1, 2, 5, 6, 23]

- the long time behavior of DG error as discussed in [5, 6, 23]. In this paper, we conclude that the error of numerical solutions at Radau points will not grow over a period of time that is on the order of Δx^{-k+1} and Δx^{-k} for DG and LDG respectively.

Moreover, supraconvergence properties of DG and LDG methods are studied based on our understanding of the eigen-structure of the amplification matrix. Extensive 1-D and 2-D numerical examples for scalar and system of equations are demonstrated to verify our analysis and to assess the superconvergence properties of DG and LDG schemes in a more general setting. Future research directions include (1) to seek an analytical proof for our symbolic analysis in this paper (2) to analyze superconvergence properties of various discontinuous Galerkin formulations.

Acknowledgement. The authors thank Prof. Chi-Wang Shu for many helpful discussions and suggestions. The research is being conducted when W. Guo and J.-M. Qiu are visiting institute of computational and experimental research in mathematics (ICERM) in Brown University. The support from ICERM is greatly appreciated. The research of the first and third author are supported by Air Force Office of Scientific Computing YIP grant FA9550-12-0318, NSF grant DMS-0914852 and DMS-1217008, University of Houston.

References

- [1] S. ADJERID, K. DEVINE, J. FLAHERTY, AND L. KRIVODONOVA, *A posteriori error estimation for discontinuous Galerkin solutions of hyperbolic problems*, Computer methods in applied mechanics and engineering, 191 (2002), pp. 1097–1112.
- [2] S. ADJERID AND T. MASSEY, *Superconvergence of discontinuous Galerkin solutions for a nonlinear scalar hyperbolic problem*, Computer methods in applied mechanics and engineering, 195 (2006), pp. 3331–3346.
- [3] M. AINSWORTH, *Dispersive and dissipative behaviour of high order discontinuous Galerkin finite element methods*, Journal of Computational Physics, 198 (2004), pp. 106–130.

- [4] M. AINSWORTH, P. MONK, AND W. MUNIZ, *Dispersive and dissipative properties of discontinuous Galerkin finite element methods for the second-order wave equation*, Journal of Scientific Computing, 27 (2006), pp. 5–40.
- [5] Y. CHENG AND C.-W. SHU, *Superconvergence and time evolution of discontinuous Galerkin finite element solutions*, Journal of Computational Physics, 227 (2008), pp. 9612–9627.
- [6] —, *Superconvergence of local discontinuous Galerkin methods for one-dimensional convection-diffusion equations*, Computers & Structures, 87 (2009), pp. 630–641.
- [7] —, *Superconvergence of discontinuous Galerkin and local discontinuous Galerkin schemes for linear hyperbolic and convection-diffusion equations in one space dimension*, SIAM Journal on Numerical Analysis, 47 (2010), pp. 4044–4072.
- [8] B. COCKBURN, F. LI, AND C.-W. SHU, *Locally divergence-free discontinuous Galerkin methods for the Maxwell equations*, Journal of Computational Physics, 194 (2004), pp. 588–610.
- [9] B. COCKBURN, M. LUSKIN, C.-W. SHU, AND E. SULI, *Enhanced accuracy by post-processing for finite element methods for hyperbolic equations*, Mathematics of Computation, 72 (2003), pp. 577–606.
- [10] B. COCKBURN AND C.-W. SHU, *Runge–Kutta discontinuous Galerkin methods for convection-dominated problems*, Journal of Scientific Computing, 16 (2001), pp. 173–261.
- [11] S. GOTTLIEB, C.-W. SHU, AND E. TADMOR, *Strong stability preserving high order time discretization methods*, SIAM Review, 43 (2001), pp. 89–112.
- [12] Y. HE, F. LI, AND J. QIU, *Dispersion and dissipation errors of two fully discrete discontinuous Galerkin methods*, submitted.
- [13] F. HU, M. HUSSAINI, AND P. RASSETARINERA, *An analysis of the discontinuous Galerkin method for wave propagation problems*, Journal of Computational Physics, 151 (1999), pp. 921–946.

- [14] G. JIANG AND C.-W. SHU, *On a cell entropy inequality for discontinuous Galerkin methods*, Mathematics of Computation, 62 (1994), pp. 531–538.
- [15] L. KRIVODONOVA AND R. QIN, *An analysis of the spectrum of the discontinuous galerkin method*, Preprint <http://www.math.uwaterloo.ca/lgk/research.html>, Submitted for publication.
- [16] Y. X. L. JI AND J. RYAN, *Accuracy-enhancement of discontinuous Galerkin solutions for convection-diffusion equations in multiple-dimensions*, Mathematics of Computation, (2012), p. to appear.
- [17] R. LOWRIE, P. ROE, AND B. VAN LEER, *A space-time discontinuous Galerkin method for the time-accurate numerical solution of hyperbolic conservation laws*, in AIAA Computational Fluid Dynamics Conference, 12 th, San Diego, CA, 1995, pp. 135–150.
- [18] T. PETERSON, *A note on the convergence of the discontinuous Galerkin method for a scalar hyperbolic equation*, SIAM Journal on Numerical Analysis, 28 (1991), pp. 133–140.
- [19] J. RYAN, C.-W. SHU, AND H. ATKINS, *Extension of a postprocessing technique for the discontinuous Galerkin method for hyperbolic equations with application to an aeroacoustic problem*, SIAM Journal on Scientific Computing, 26 (2005), pp. 821–843.
- [20] D. SÁRMÁNY, M. BOTCHEV, AND J. VAN DER VEGT, *Dispersion and dissipation error in high-order Runge-Kutta discontinuous Galerkin discretisations of the Maxwell equations*, Journal of Scientific Computing, 33 (2007), pp. 47–74.
- [21] S. SHERWIN, *Dispersion analysis of the continuous and discontinuous Galerkin formulation*, Lecture Notes in Computational Science and Engineering, 11 (2000), pp. 425–432.
- [22] Y. XU AND C. SHU, *Local discontinuous galerkin methods for high-order time-dependent partial differential equations*, Communications in Computational Physics, v7, (2010), pp. 1–46.

- [23] Y. YANG AND C.-W. SHU, *Superconvergence of discontinuous Galerkin method for linear hyperbolic equations in one space dimension*, SIAM Journal on Numerical Analysis, submitted (2012).
- [24] M. ZHANG AND C. SHU, *An analysis of and a comparison between the discontinuous Galerkin and the spectral finite volume methods*, Computers & fluids, 34 (2005), pp. 581–592.
- [25] M. ZHANG AND C.-W. SHU, *An analysis of three different formulations of the discontinuous Galerkin method for diffusion equations*, Mathematical Models and Methods in Applied Sciences, 13 (2003), pp. 395–413.
- [26] X. ZHONG AND C.-W. SHU, *Numerical resolution of discontinuous Galerkin methods for time dependent wave equations*, Computer Methods in Applied Mechanics and Engineering, 200 (2011), pp. 2814–2827.